Electronic Supplementary Information for Dalton Transactions

Supporting Information (SI)

Heteroditopic ligands based on ferrocenyl benzimidazoles fused to an additional diaza heterocyclic ring system

María Alfonso, Antonia Sola, Antonio Caballero, Alberto Tárraga, * and Pedro Molina*

Departamento de Química Orgánica. Facultad de Química. Universidad de Murcia. Campus de Espinardo, E-30100 Murcia, Spain.

E-mail: pmolina@um.es; atarraga@um.es

Table of contents

7-Ferrocenyl-*8H*-imidazo [4,5-*e*]-2,1,2-benzothiadiazole, [2]

^{1}H NMR (200MHz, DMSO)

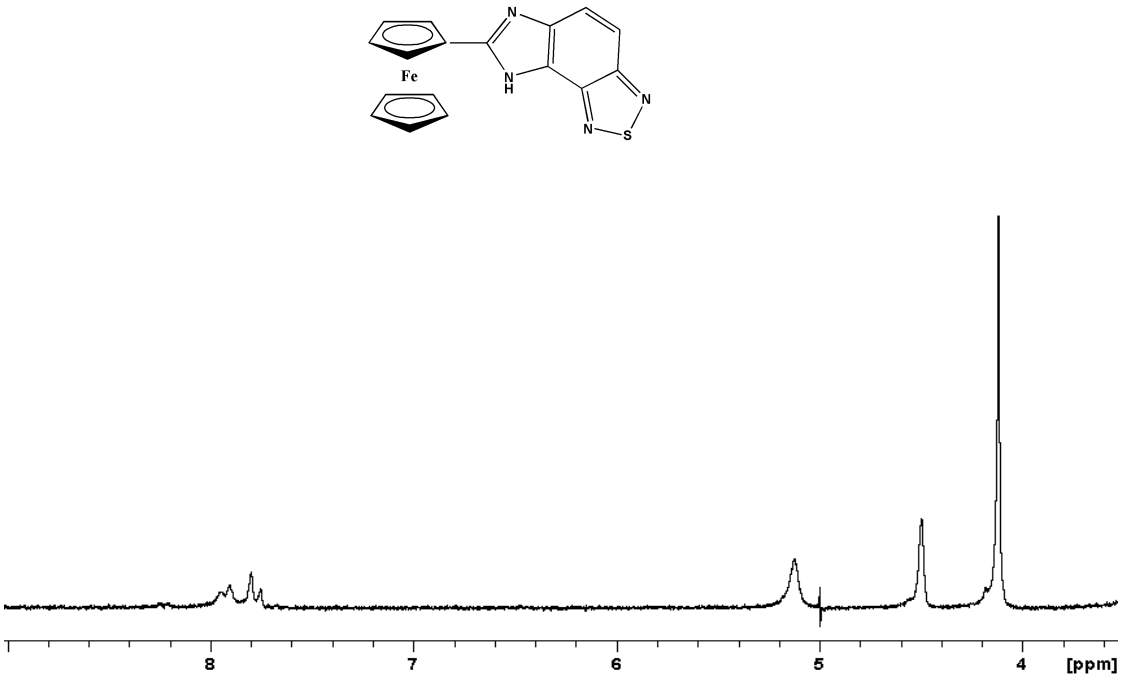

^{13}C NMR (50 MHz, DMSO)

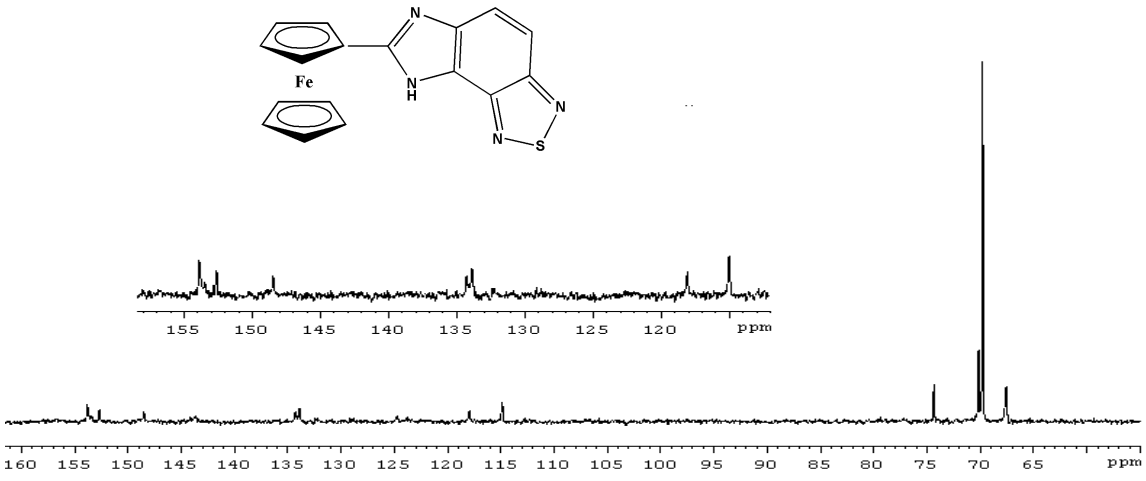

2-Ferrocenyl-*3H*-imidazo [4,5-*f*]quinoxaline, [3]

H NMR (300 MHz, CD_3OD):]

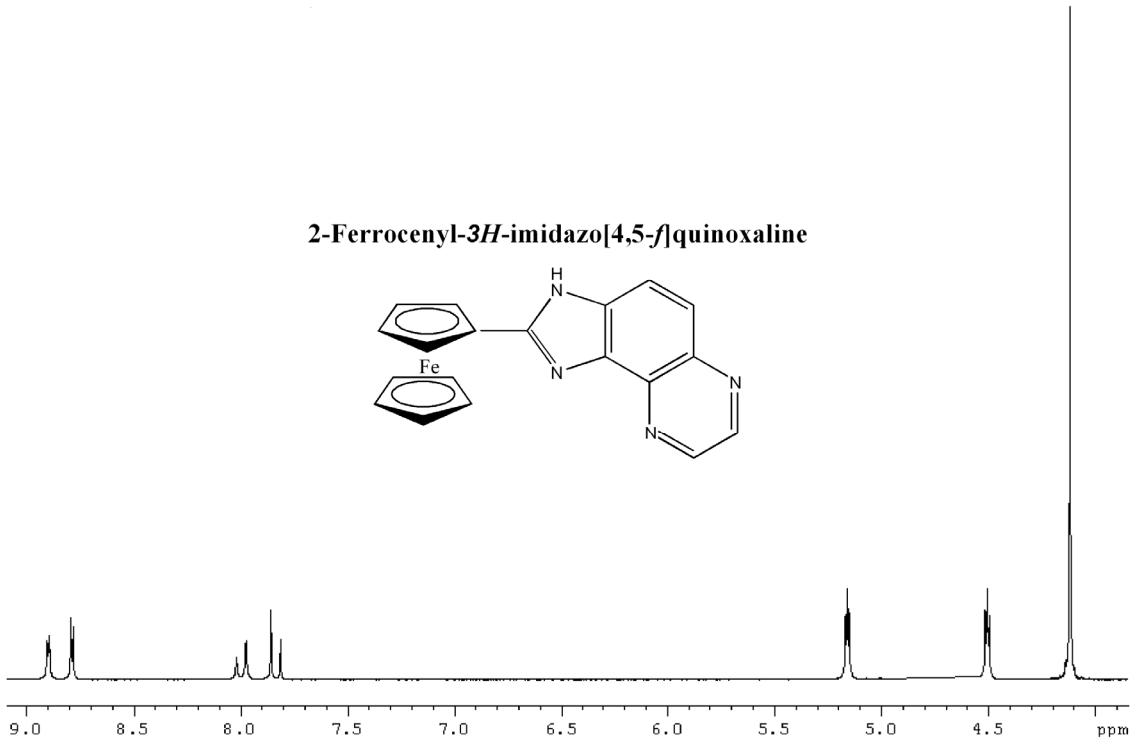

^{13}C NMR (75 MHz, CD_3OD):

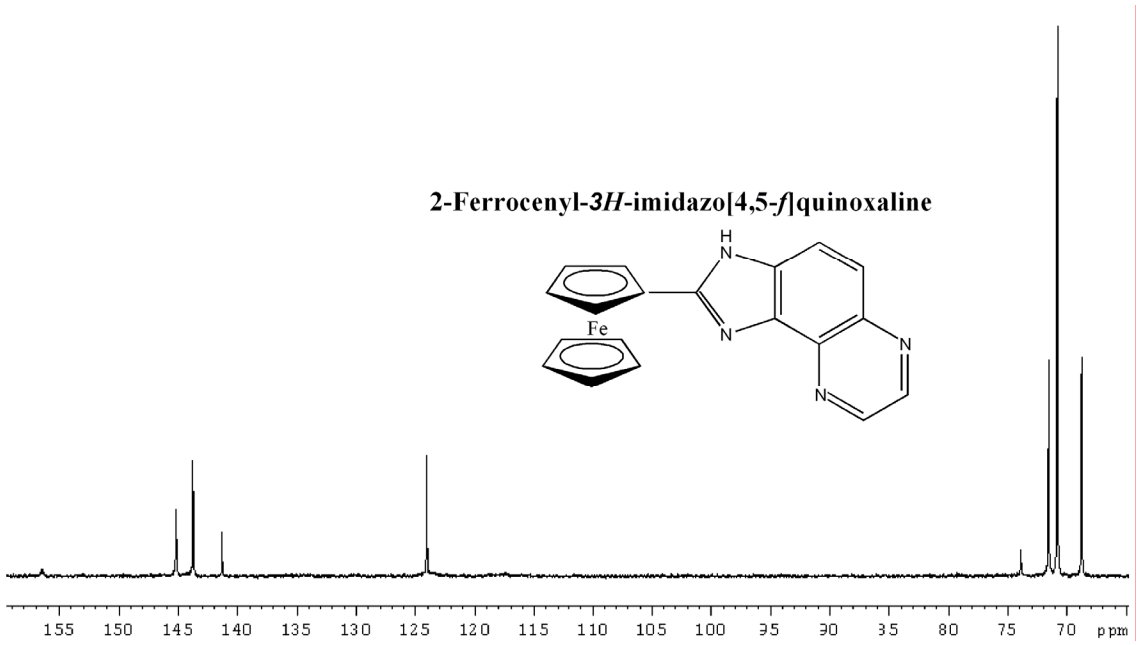

Table S1. Electrochemical data of the receptors **2** and **3** and their metal complexes formed

Comp.	$E_{1/2}$(mV)	ΔE(mV)[a]	K_{red}/K_{ox} (BEF)[b]
2	520	-	-
2·Pb^{2+}	720	200	2800
3·	580	-	
3·Cd^{2+}	650	73	17
3·Zn^{2+}	670	88	31
3·Hg^{2+}	730	150	340
3·Pb^{2+}	650	67	13

a) $\Delta E = E_{1/2}$ (complex) - $E_{1/2}$ (free ligand); b) BEF = Binding Enhancement Factor, calculated using the equation $\ln(K_{red}/K_{ox}) = \Delta E°(nF/RT)$, where the equilibrium constants K_{ox} and K_{red} correspond to the complexation processes by the oxidized and reduced form of the ligand

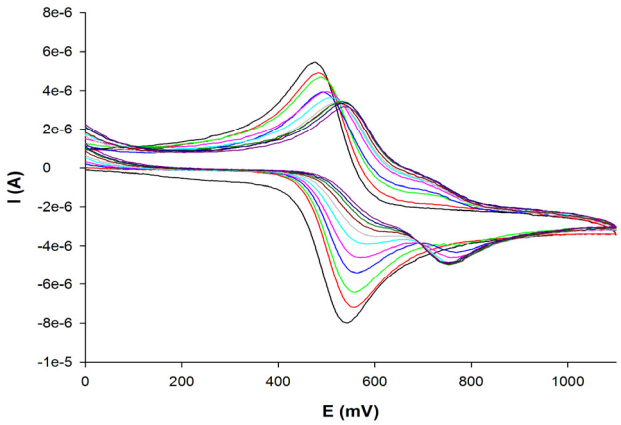

Figure SI 1. Evolution of the CV of **2** (1 mM) in $CH_3CN/[(n\text{-}Bu)_4]ClO_4$ scanned at 0.1 V s^{-1} in the presence of increasing amounts of Pb^{2+}: the initial (black) is that of **2** and the final one (purple), after addition of 1 equivalent of Pb^{2+}.

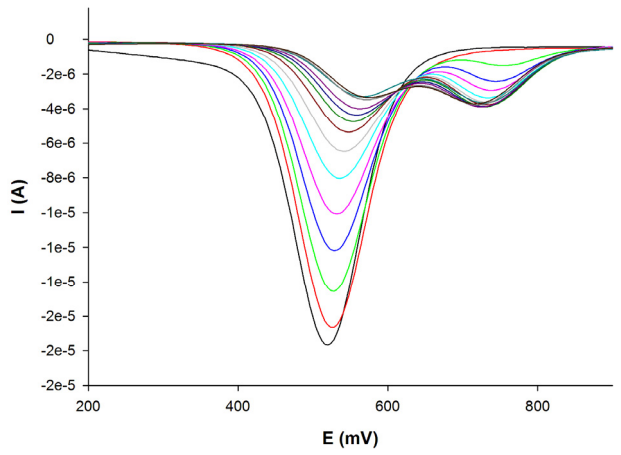

Figure SI 2. Evolution of the SWV of **2** (1 mM) in $CH_3CN/[(n\text{-}Bu)_4]ClO_4$ scanned at 0.1 V s^{-1} in the presence of increasing amounts of Pb^{2+}: the initial (black) is that of **2** and the final one (purple), after addition of 1 equivalent of Pb^{2+}.

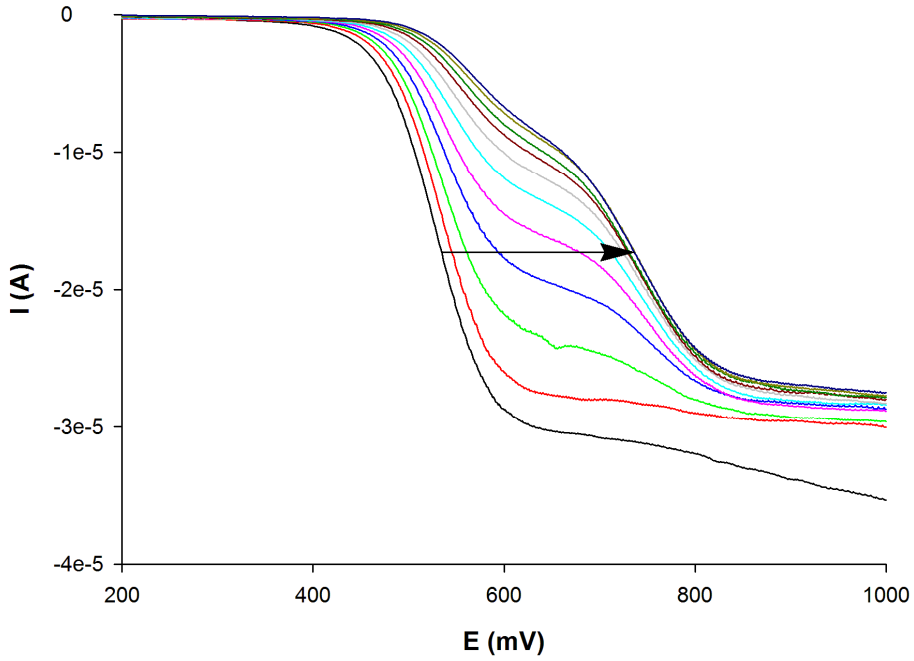

Figure SI 3. Evolution of the LSW in the presence of increasing amounts of Pb^{+2}: the initial (black) is that of **2** (1 mM) and the final one (deep blue), after addition of 1 equivalent of Pb^{+2}, $[(n\text{-}Bu)_4]ClO_4$ 0.1 M as supporting electrolyte, obtained using a rotating disk electrode at 100 mVs^{-1} and 1000 rpm.

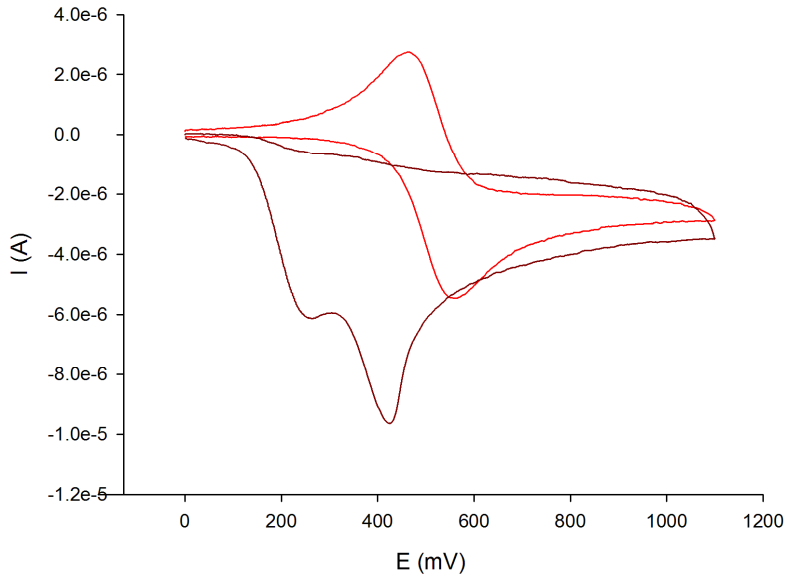

Figure SI 4. CV of **2** (red) (1 mM) in $CH_3CN/[(n\text{-}Bu)_4]ClO_4$ scanned at 0.1 V s^{-1} and in the presence 1 equiv of $HP_2O_7^{-3}$ (purple).

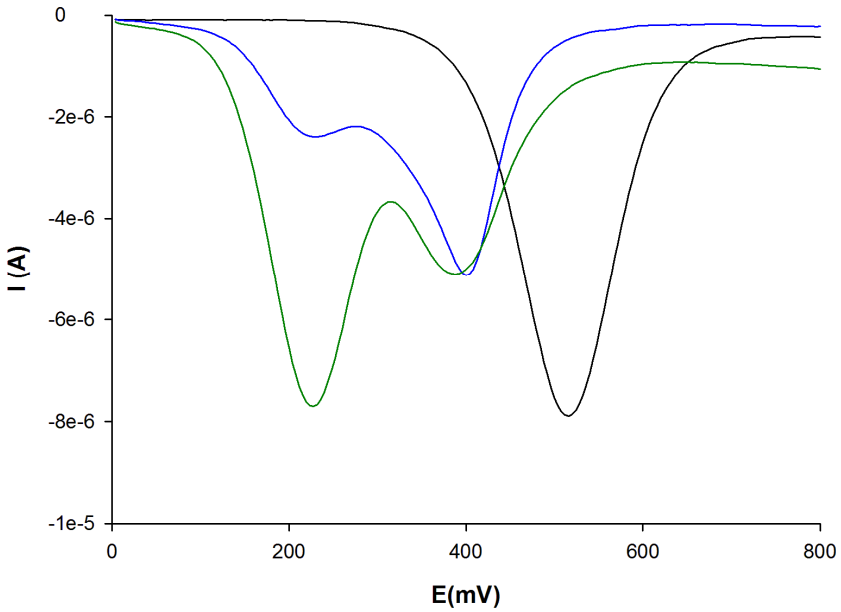

Figure SI 5. SWV of **2** (black) (1 mM) in CH_3CN/[(*n*-Bu)$_4$]ClO_4 scanned at 0.1 V s^{-1} and in the presence 0.4 equiv of $HP_2O_7^{-3}$ (blue) and in the presence 1.6 equiv of $HP_2O_7^{-3}$ (green).

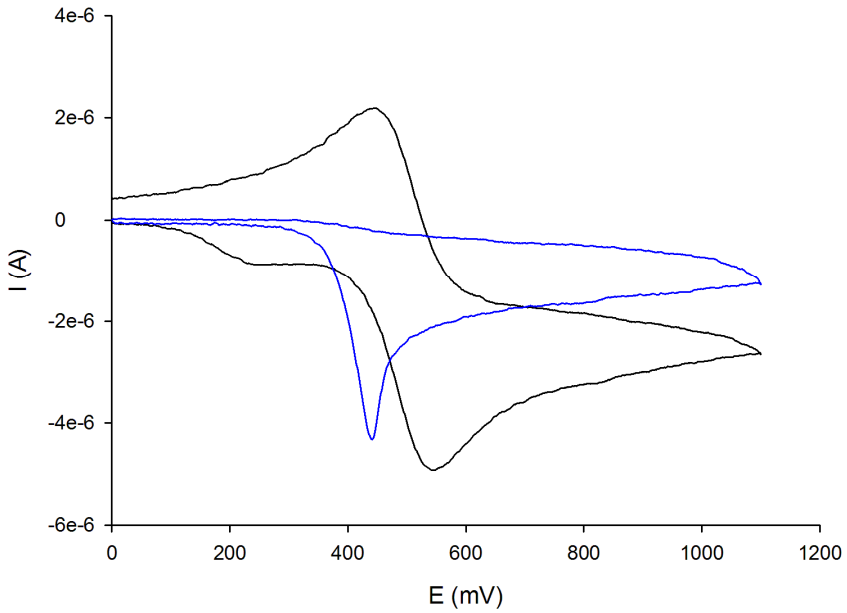

Figure SI 6. CV of **2** (black) (1 mM) in CH_3CN/[(*n*-Bu)$_4$]ClO_4 scanned at 0.1 V s^{-1} and in the presence 1 equiv of $HP_2O_7^{-3}$ (blue) and 20 equiv of acetic acid in CH_3CN.

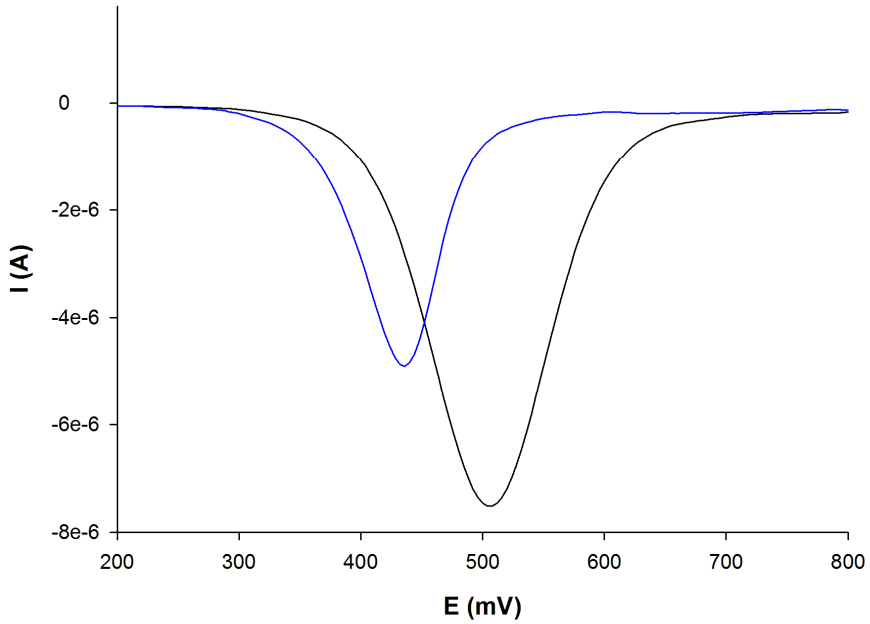

Figure SI 7. SWV of **2** (black) (1 mM) in $CH_3CN/[(n\text{-}Bu)_4]ClO_4$ scanned at 0.1 V s^{-1} and in the presence 2 equiv of $HP_2O_7^{-3}$ (blue) and 20 equiv of acetic acid in CH_3CN.

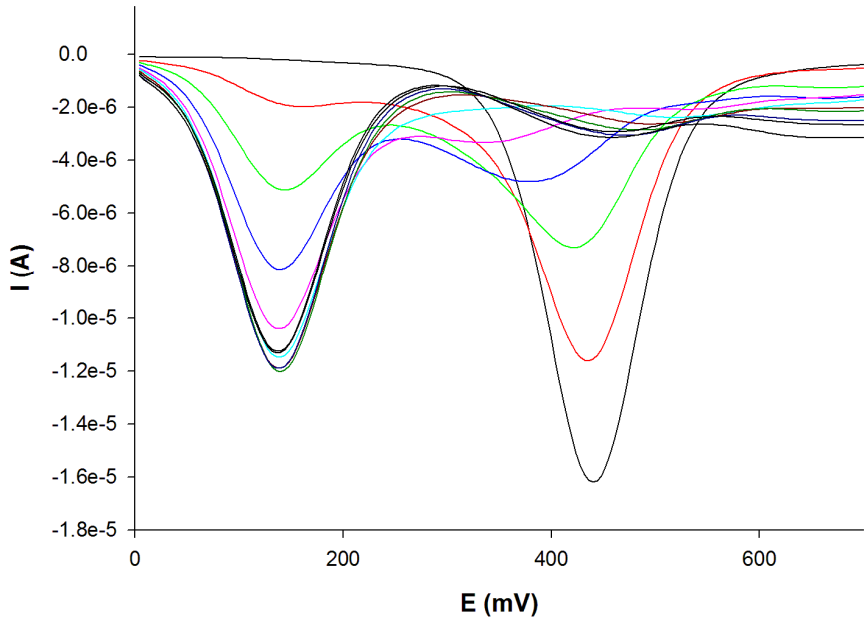

Figure SI 8. Evolution of the OSWV of **2** (1 mM) in $CH_3CN/[(n\text{-}Bu)_4]ClO_4$ scanned at 0.1 V s^{-1} in the presence of increasing amounts of F^-: the initial (black) is that of **2** and the final one (deep green), after addition of 5 equivalent of F^-.

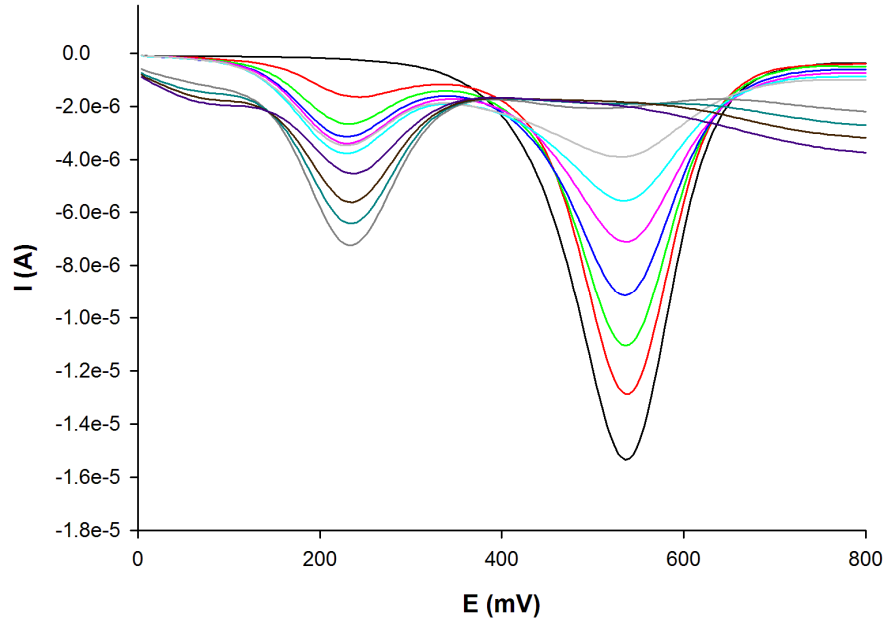

Figure SI 9. Evolution of the OSWV of **2** (1 mM) in $CH_3CN/[(n\text{-}Bu)_4]ClO_4$ scanned at 0.1 V s^{-1} in the presence of increasing amounts of OH^-: the initial (black) is that of **2** and the final one (gray), after addition of 2 equivalent of OH^-.

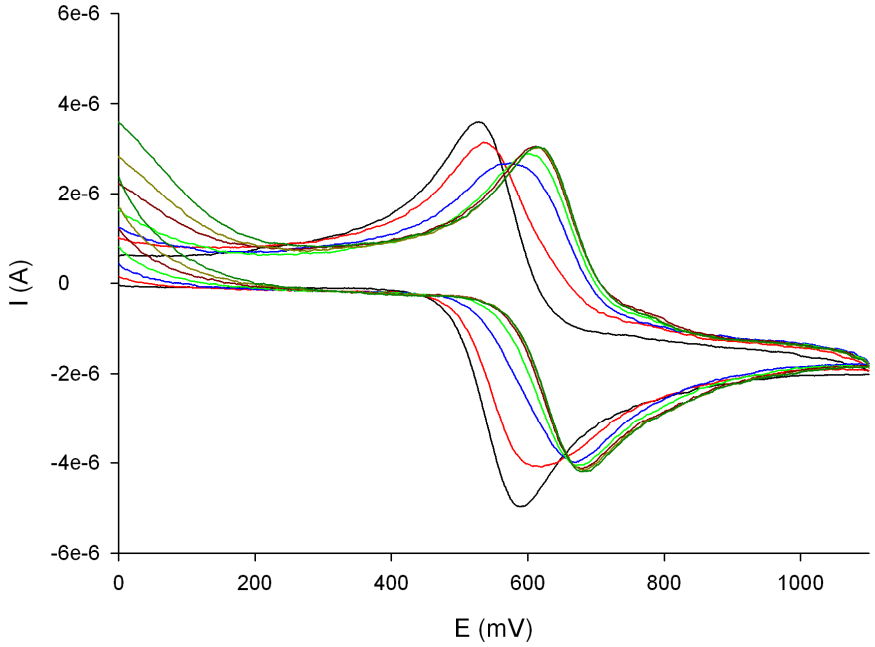

Figure SI 10. Evolution of the CV of **3** (1 mM) in $CH_3CN/[(n\text{-}Bu)_4]ClO_4$ scanned at 0.1 V s^{-1} in the presence of increasing amounts of Pb^{2+}: the initial (black) is that of **3** and the final one (deep green), after addition of 0.5 equivalent of Pb^{2+}.

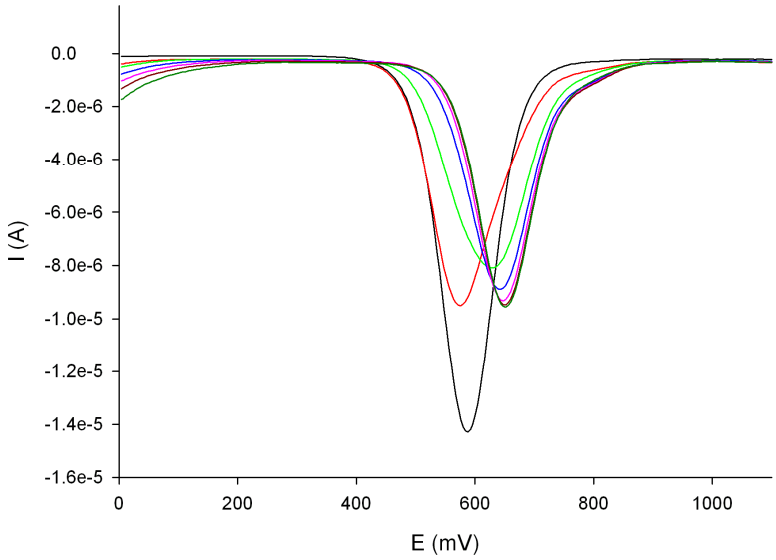

Figure SI 11. Evolution of the OSWV of **3** (1 mM) in $CH_3CN/[(n\text{-}Bu)_4]ClO_4$ scanned at 0.1 V s^{-1} in the presence of increasing amounts of Pb^{2+}: the initial (black) is that of **3** and the final one (deep green), after addition of 0.5 equivalent of Pb^{2+}.

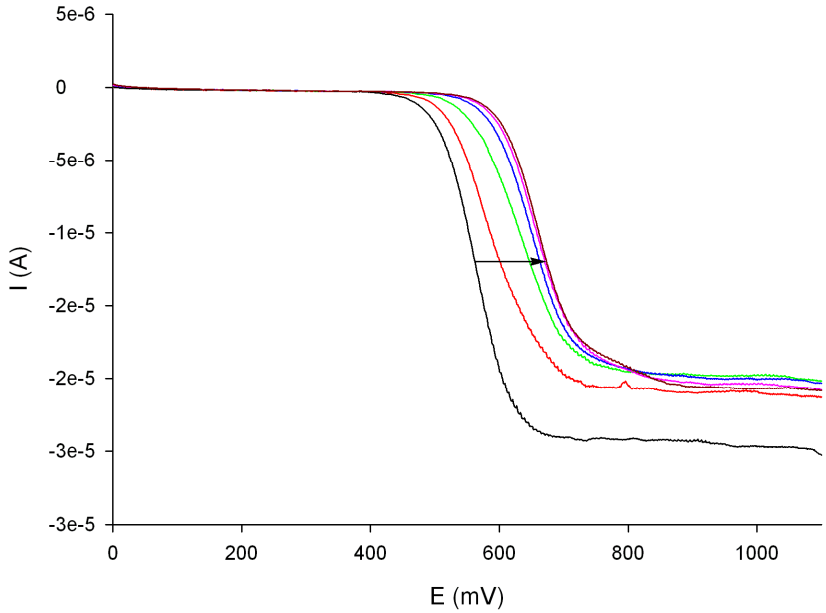

Figure SI 12. Evolution of the LSW in the presence of increasing amounts of Pb^{2+}: the initial (black) is that of **3** (1 mM in CH_3CN) and the final one (deep red), after addition of 0.5 equivalent of Pb^{2+}, $[(n\text{-}Bu)_4]ClO_4$ 0.1 M as supporting electrolyte, obtained using a rotating disk electrode at 100 mVs^{-1} and 1000 rpm.

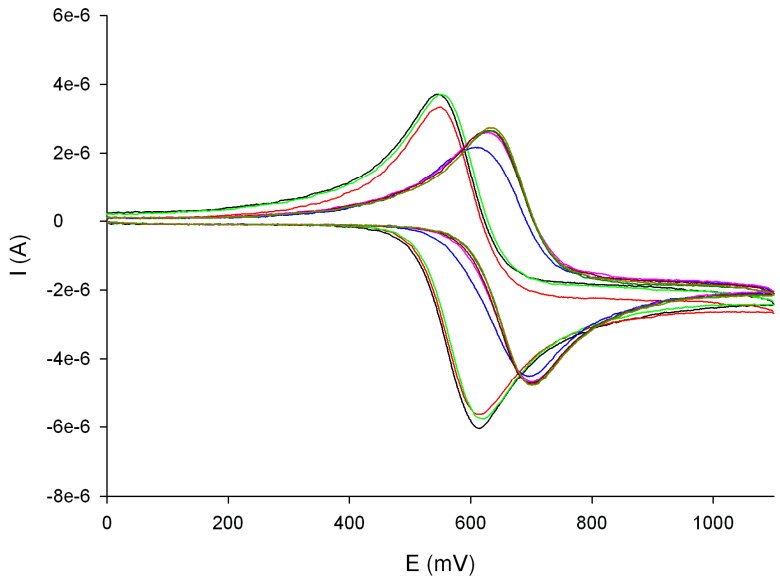

Figure SI 13. Evolution of the CV of **3** (1 mM) in $CH_3CN/[(n\text{-}Bu)_4]ClO_4$ scanned at 0.1 V s^{-1} in the presence of increasing amounts of Zn^{2+}: the initial (black) is that of **3** and the final one (deep yellow), after addition of 1 equivalent of Zn^{2+}.

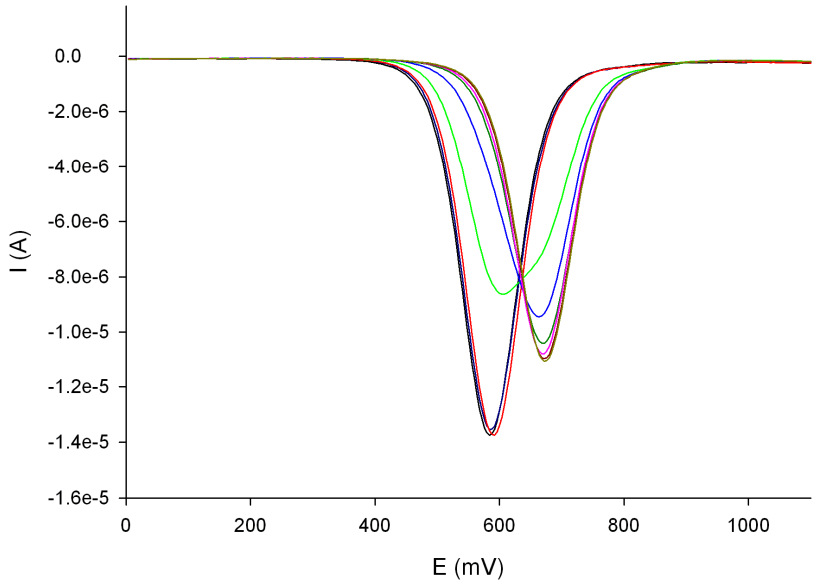

Figure SI 14. Evolution of the OSWV of **3** (1 mM) in $CH_3CN/[(n\text{-}Bu)_4]ClO_4$ scanned at 0.1 V s^{-1} in the presence of increasing amounts of Zn^{2+}: the initial (black) is that of **3** and the final one (deep yellow), after addition of 1 equivalent of Zn^{2+}.

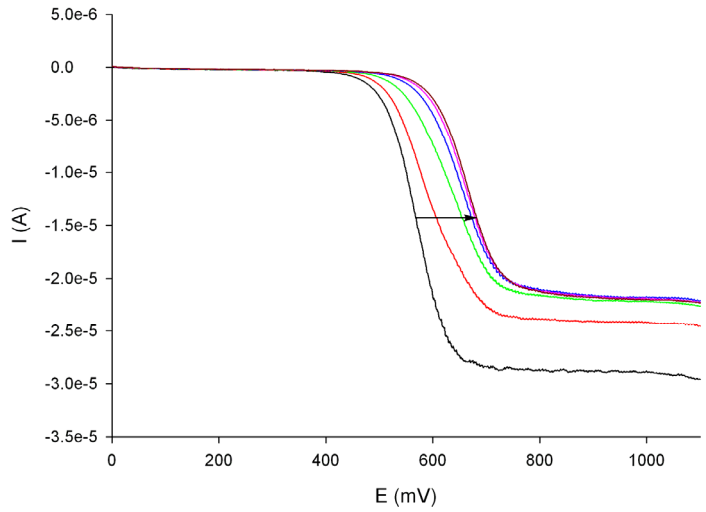

Figure SI 15. Evolution of the LSW in the presence of increasing amounts of Zn^{2+}: the initial (black) is that of **3** (1 mM in CH_3CN) and the final one (deep red), after addition of 1 equivalent of Zn^{2+} $[(n\text{-}Bu)_4]ClO_4$ 0.1 M as supporting electrolyte, obtained using a rotating disk electrode at 100 mVs^{-1} and 1000 rpm.

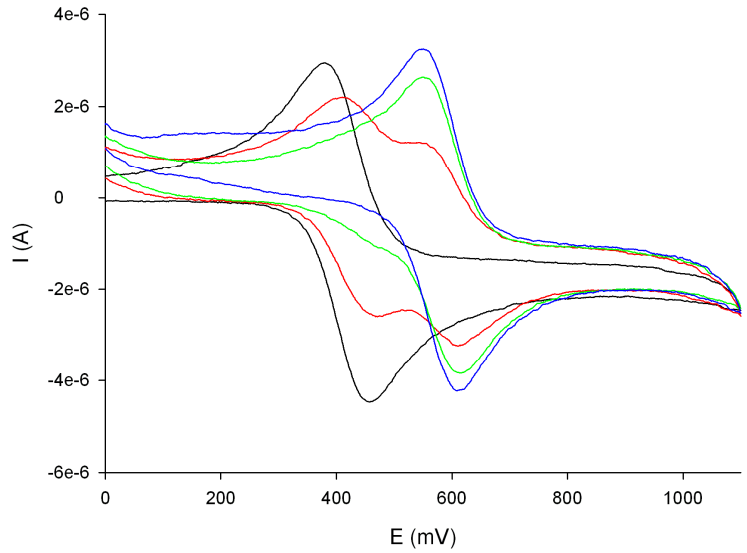

Figure SI 16. Evolution of the CV of **3** (1 mM) in $CH_3CN/[(n\text{-}Bu)_4]ClO_4$ scanned at 0.1 V s^{-1} in the presence of increasing amounts of Hg^{2+}: the initial (black) is that of **3** and the final one (blue), after addition of 0.5 equivalent of Hg^{2+}.

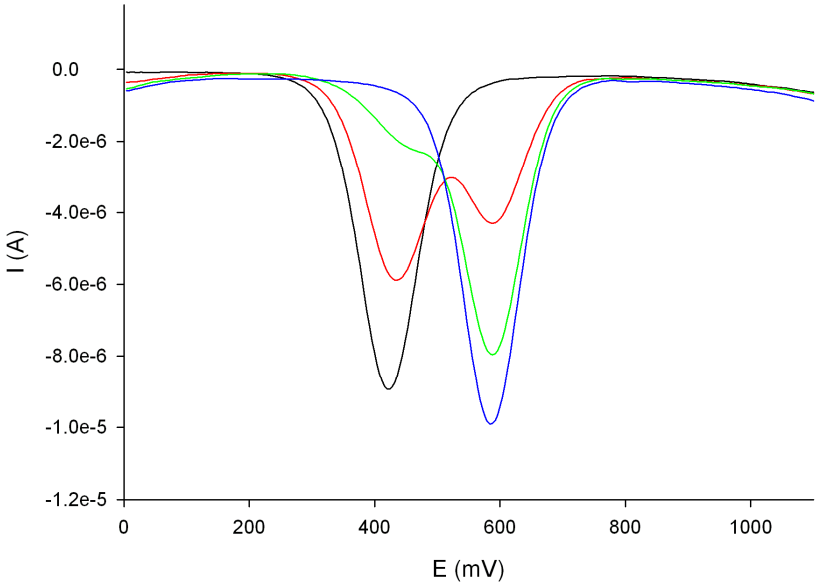

Figure SI 17. Evolution of the OSWV of **3** (1 mM) in $CH_3CN/[(n\text{-}Bu)_4]ClO_4$ scanned at 0.1 V s^{-1} in the presence of increasing amounts of Hg^{2+}: the initial (black) is that of **3** and the final one (blue), after addition of 0.5 equivalent of Hg^{2+}.

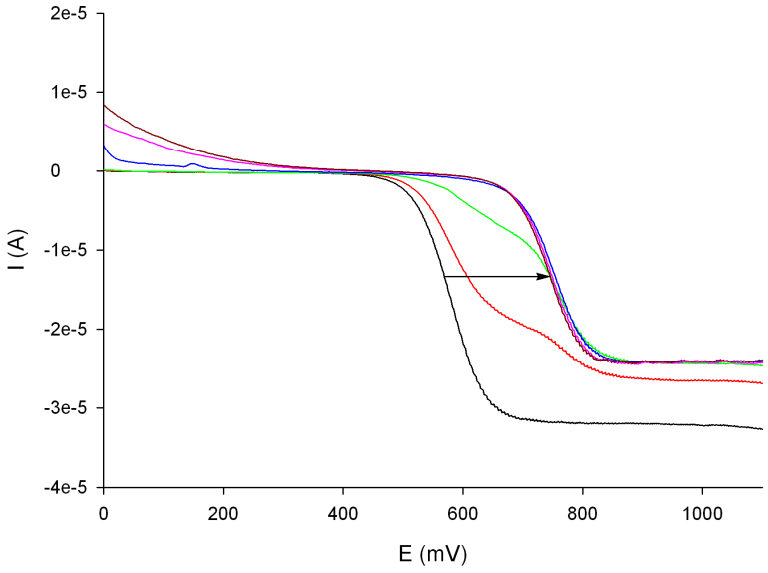

Figure SI 18. Evolution of the LSW in the presence of increasing amounts of Hg^{2+}: the initial (black) is that of **3** (1 mM in CH_3CN) and the final one (deep red), after addition of 0.5 equivalent of Hg^{2+} $[(n\text{-}Bu)_4]ClO_4$ 0.1 M as supporting electrolyte, obtained using a rotating disk electrode at 100 mVs^{-1} and 1000 rpm.

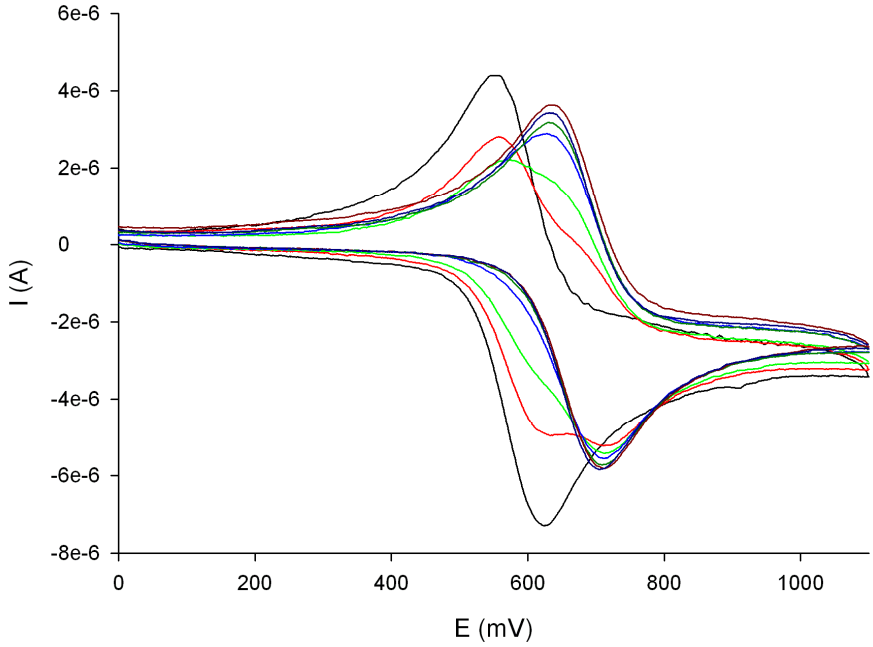

Figure SI 19. Evolution of the CV of **3** (1 mM) in $CH_3CN/[(n\text{-}Bu)_4]ClO_4$ scanned at 0.1 V s^{-1} in the presence of increasing amounts of Cd^{2+}: the initial (black) is that of **3** and the final one (deep blue), after addition of 1 equivalent of Cd^{2+}.

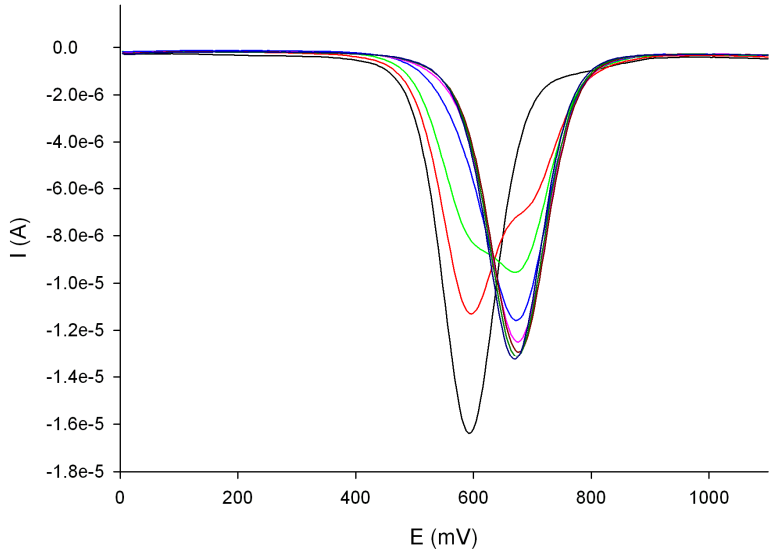

Figure SI 20. Evolution of the OSWV of **3** (1 mM) in $CH_3CN/[(n\text{-}Bu)_4]ClO_4$ scanned at 0.1 V s^{-1} in the presence of increasing amounts of Cd^{2+}: the initial (black) is that of **3** and the final one (deep blue), after addition of 1 equivalent of Cd^{2+}.

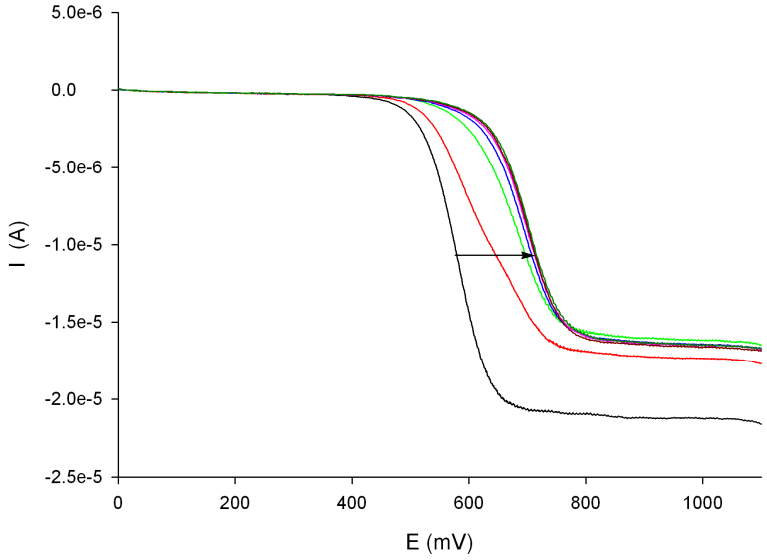

Figure SI 21. Evolution of the LSW in the presence of increasing amounts of Cd^{2+}: the initial (black) is that of **3** (1 mM in CH_3CN) and the final one (deep red), after addition of 1 equivalent of Cd^{2+}, $[(n\text{-}Bu)_4]ClO_4$ 0.1 M as supporting electrolyte, obtained using a rotating disk electrode at 100 mVs^{-1} and 1000 rpm.

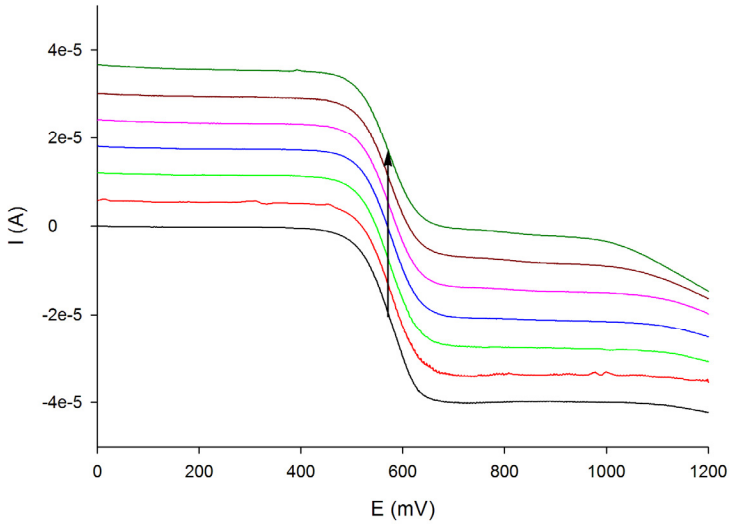

Figure SI 22. Evolution of the LSW in the presence of increasing amounts of Cu^{2+}: the initial (black) is that of **3** and the final one (deep green), after addition of 2 equivalents of Cu^{2+} $[(n\text{-}Bu)_4]ClO_4$ 0.1 M as supporting electrolyte, obtained using a rotating disk electrode at 100 mVs^{-1} and 1000 rpm.

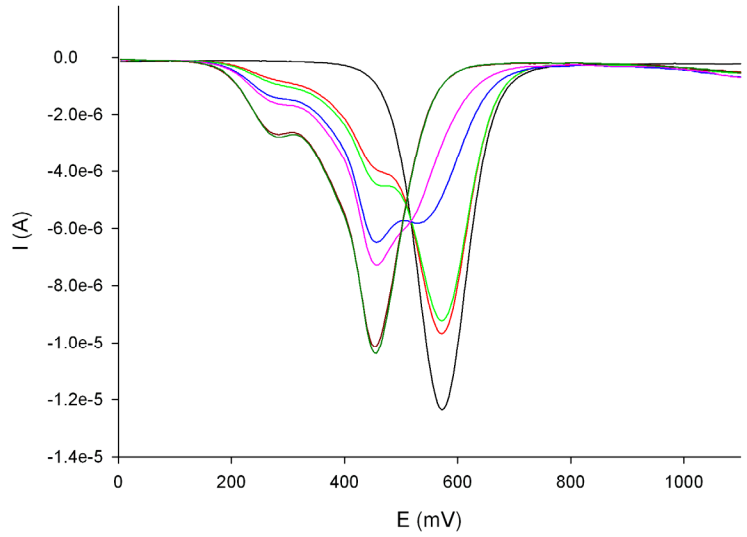

Figure SI 23. Evolution of the OSWV of **3** (1 mM) in $CH_3CN/[(n\text{-}Bu)_4]ClO_4$ scanned at 0.1 V s^{-1} in the presence of increasing amounts of $HP_2O_7^{3-}$: the initial (black) is that of **3** and the final one (deep green), after addition of 3 equivalent of $HP_2O_7^{3-}$.

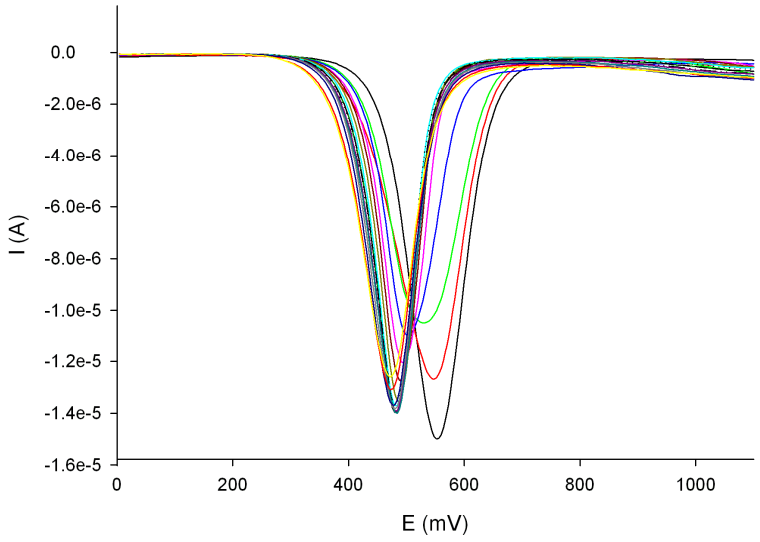

Figure SI 24. Evolution of the OSWV of **3** (1 mM) in $CH_3CN/[(n\text{-}Bu)_4]ClO_4$ in the presence of 20 mM AcOH, scanned at 0.1 V s^{-1} upon addition of increasing amounts of $HP_2O_7^{3-}$ the initial (black) is that of **3** and the final one (deep pink), after addition of 3 equivalents of $HP_2O_7^{3-}$.

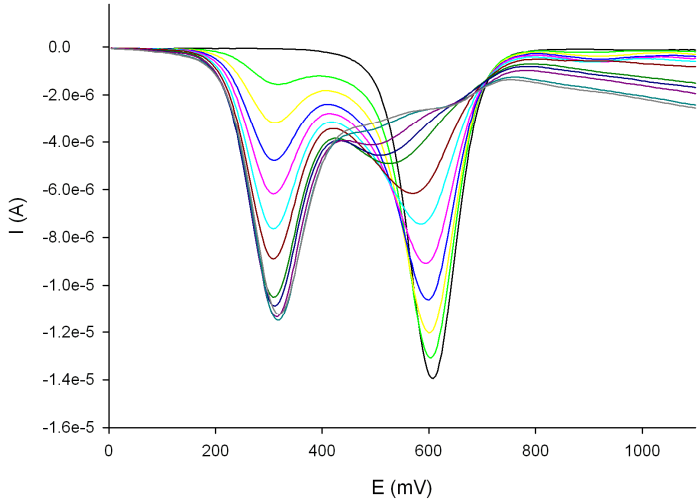

Figure SI 25. Evolution of the OSWV of **3** (1 mM) in $CH_3CN/[(n\text{-}Bu)_4]ClO_4$ scanned at 0.1 V s^{-1} in the presence of increasing amounts of F^-: the initial (black) is that of **3** and the final one (deep gray), after addition of 2 equivalents of F^-.

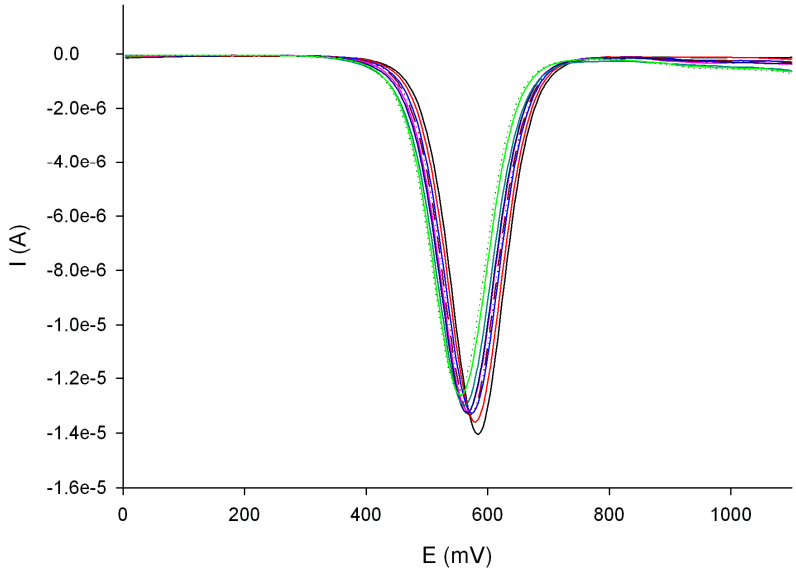

Figure SI 26. Evolution of the OSWV of **3** (1 mM) in $CH_3CN/[(n\text{-}Bu)_4]ClO_4$ in the presence of 20 mM AcOH, scanned at 0.1 V s^{-1} upon addition of increasing amounts of $HP_2O_7^{3-}$ the initial (black) is that of **3** and the final one (green), after addition of 2 equivalents of F^-.

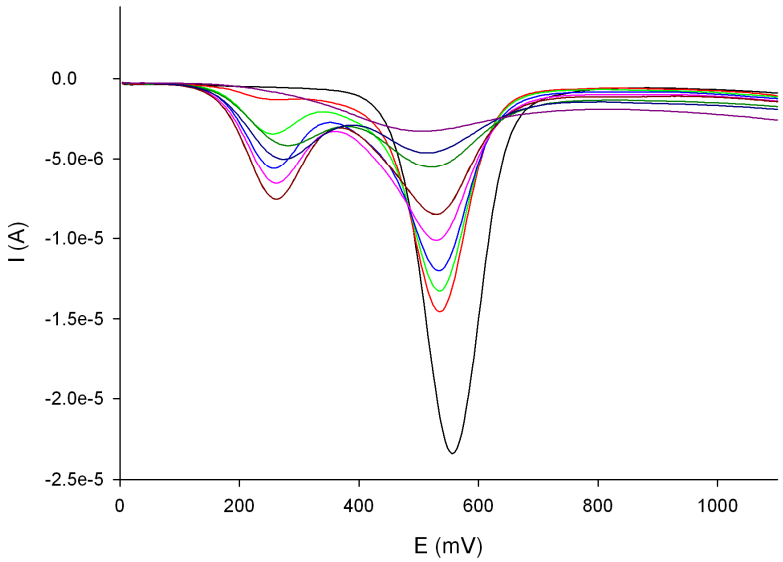

Figure SI 27. Evolution of the OSWV of **3** (1 mM) in $CH_3CN/[(n\text{-}Bu)_4]ClO_4$ scanned at 0.1 V s^{-1} in the presence of increasing amounts of OH^-: the initial (black) is that of **3** and the final one (deep red), after addition of 2 equivalents of OH^-.

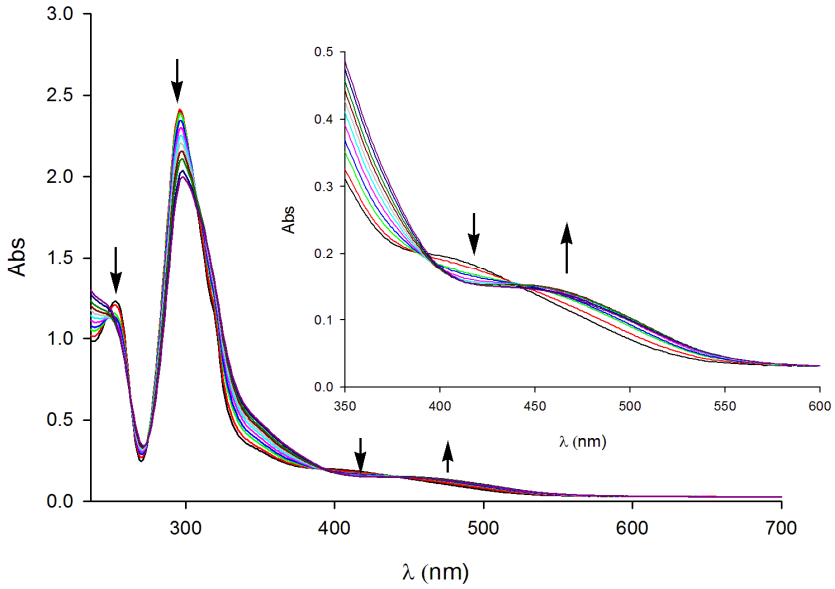

Figure SI 28. Changes in the absorption spectra of **2** (black) ($c = 1 \cdot 10^{-4}$M in CH_3CN) upon addition of increasing amounts of Pb^{2+} metal cation, until 1 equiv was added (purple). Arrows indicate absorption that increase or decrease during the experiment.

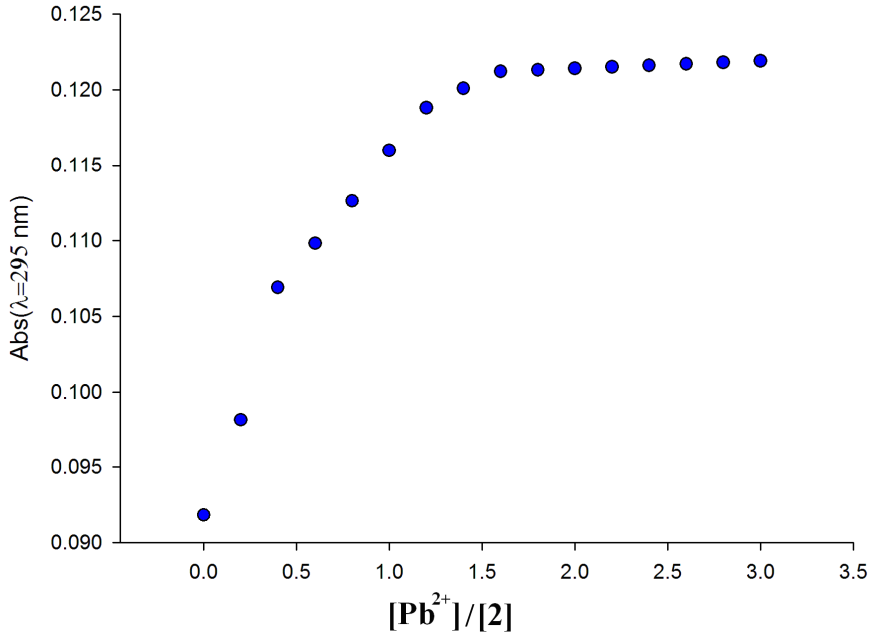

Figure SI 29. Change of absorbance of **2** (c = $1 \cdot 10^{-4}$M in CH_3CN) at λ = 295 nm upon addition of Pb^{2+}, indicating the formation of 1:1 complex.

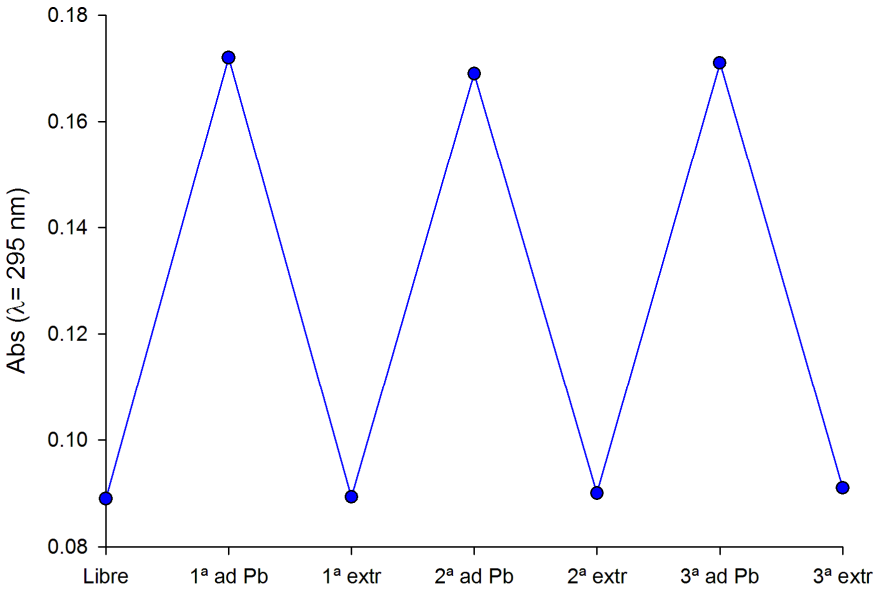

Figure SI 30. Stepwise complexation (addition of Pb^{2+}) /decomplexation (extraction with H_2O) cycles of ligand **2** ($1 \cdot 10^{-4}$ M in CH_2Cl_2) and Pb^{2+}, carried out by UV/Vis analysis.

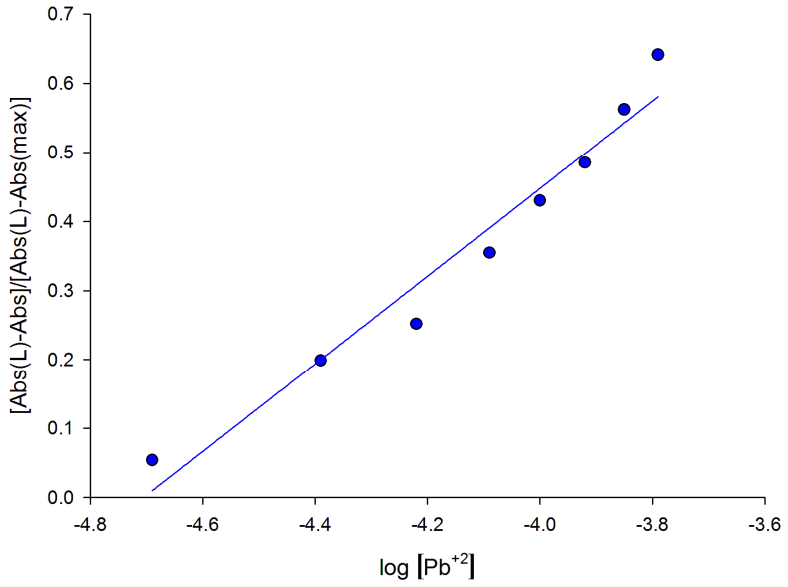

Figure SI 31. Absorbance of **2** (c = $1 \cdot 10^{-4}$M in CH_3CN) at each concentration of Pb^{2+} added, normalized between the minimum absorbance, found at zero equiv of Pb^{2+}; and the maximum absorbance, found at $[Pb^{2+}]=2 \cdot 10^{-5}$ M.

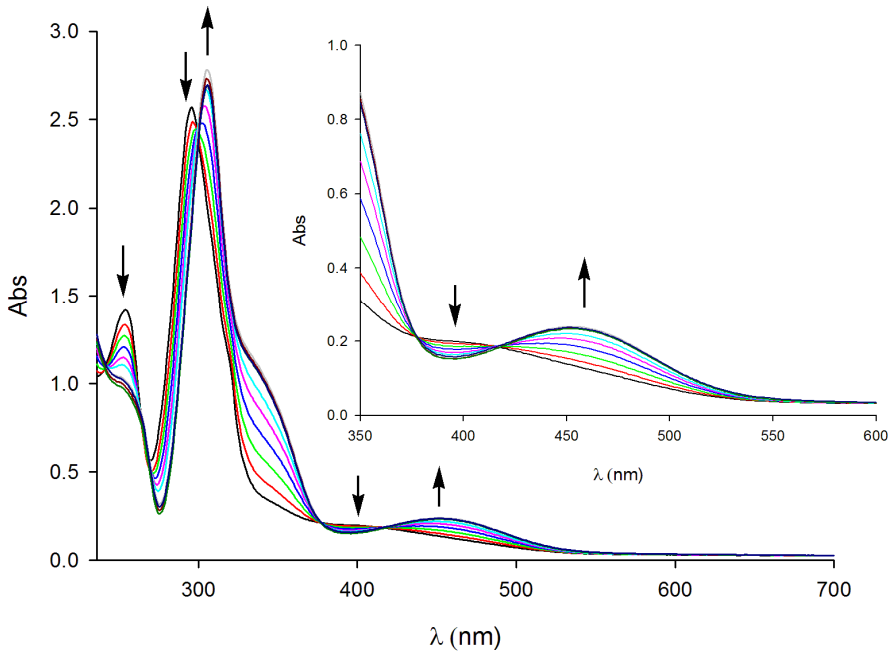

Figure 32. Changes in the absorption spectra of **2** (black) (c = $1 \cdot 10^{-4}$M in CH_3CN) upon addition of increasing amounts of $HP_2O_7^{-3}$ anion, until 1 equiv was added (gray). Arrows indicate absorption that increase or decrease during the experiment.

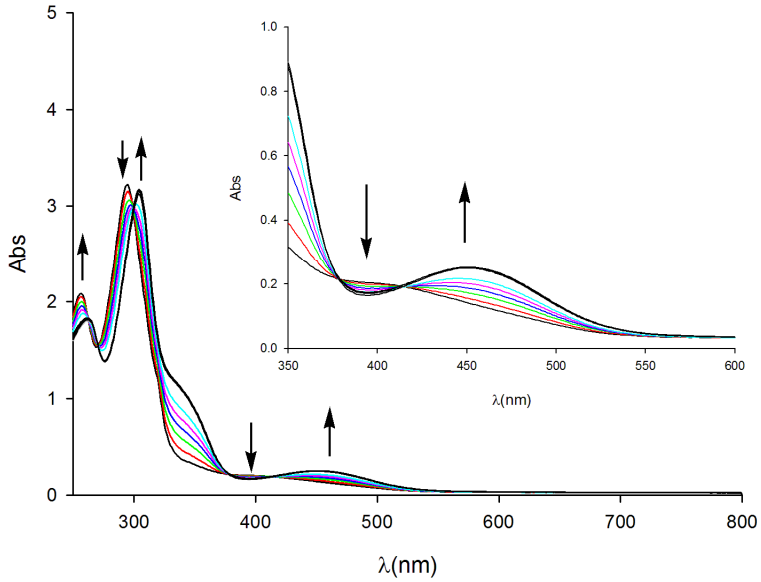

Figure SI 33. Changes in the absorption spectra of **2** (black) (c = $1 \cdot 10^{-4}$M in CH_3CN) upon addition of increasing amounts of OH^- anion, until 1 equiv was added (gray). Arrows indicate absorption that increase or decrease during the experiment.

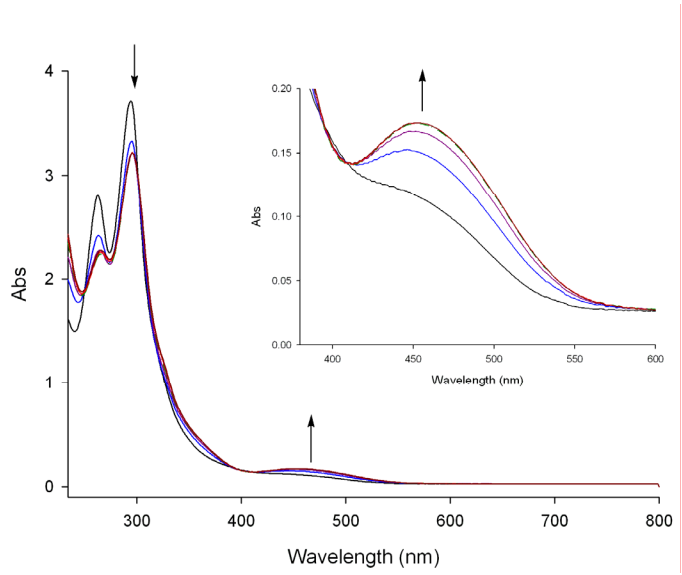

Figure SI 34. Changes in the absorption spectra of **3** (black) (c = $1 \cdot 10^{-4}$M in CH_3CN) upon addition of increasing amounts of Pb^{2+} metal cation, until 0.5 equiv was added (deep red). Arrows indicate absorption that increase or decrease during the experiment.

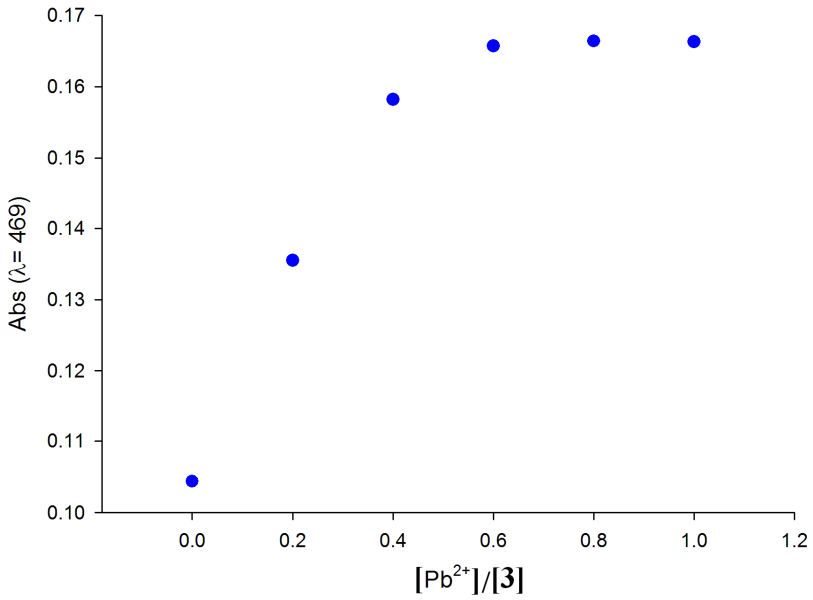

Figure SI 35. Change of absorbance of **3** (c = $1 \cdot 10^{-4}$M in CH_3CN) at λ = 469 nm upon addition of Pb^{2+}, indicating the formation of 2:1 complex.

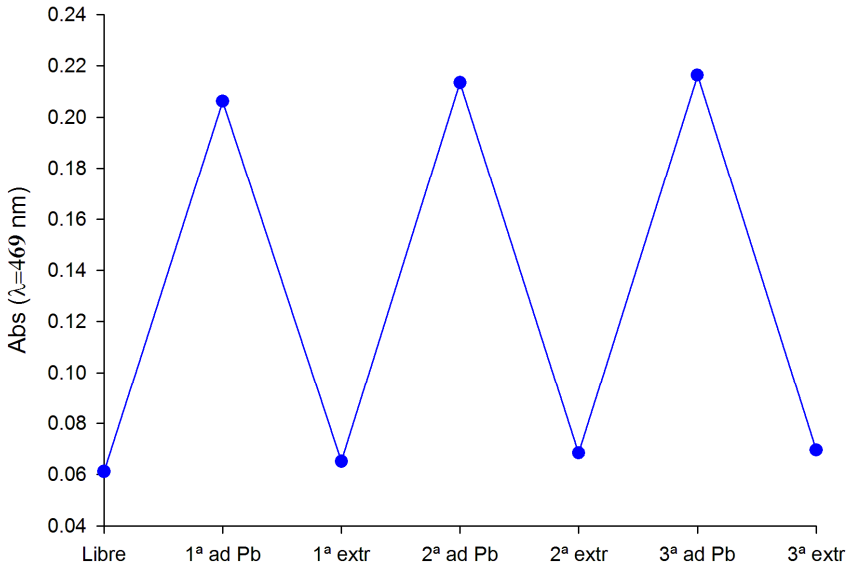

Figure SI 36. Stepwise complexation (addition of Pb^{2+}) /decomplexation (extraction with H_2O) cycles of ligand **3** (c = $1 \cdot 10^{-4}$M in CH_3CN) and Pb^{2+}, carried out by UV/Vis analysis.

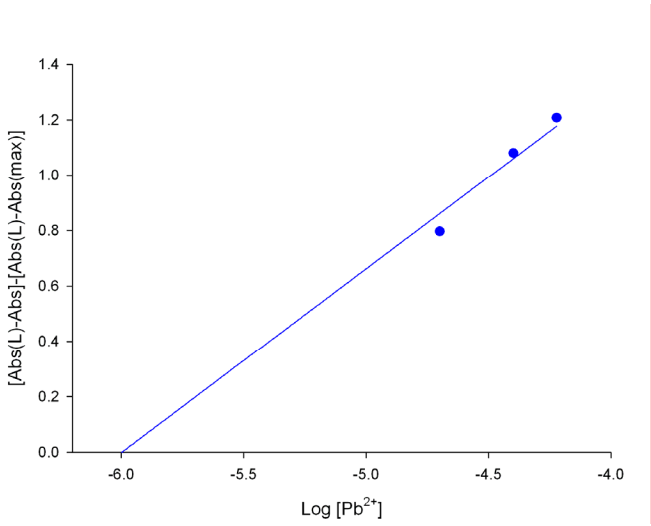

Figure SI 37. Absorbance of **3** (c = $1 \cdot 10^{-4}$M in CH_3CN) at each concentration of Pb^{2+} added, normalized between the minimum absorbance, found at zero equiv of Pb^{2+}; and the maximum absorbance, found at $[Pb^{2+}]= 1.0035 \cdot 10^{-6}$ M.

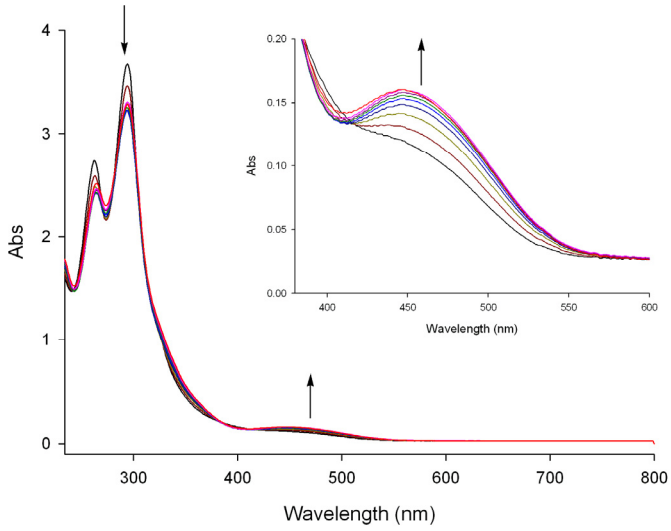

Figure SI 38. Changes in the absorption spectra of **3** (black) (c = $1 \cdot 10^{-4}$M in CH_3CN) upon addition of increasing amounts of Zn^{2+} metal cation, until 1 equiv was added (red). Arrows indicate absorption that increase or decrease during the experiment.

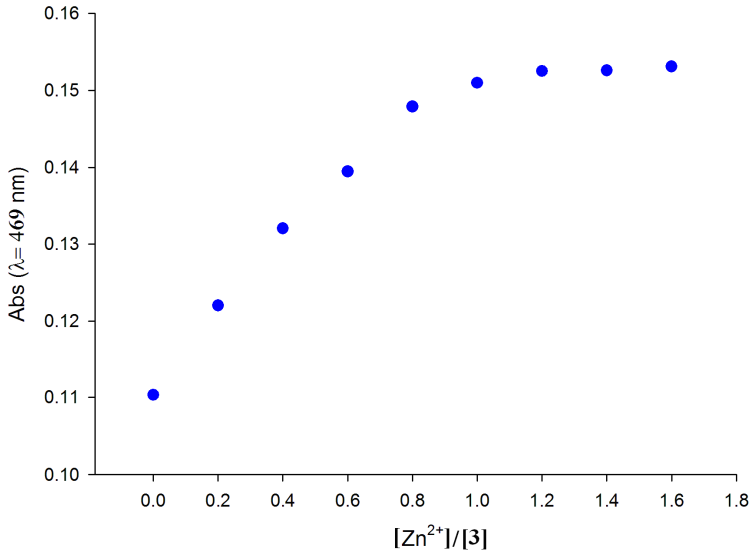

Figure SI 39. Change of absorbance of **3** (c = $1 \cdot 10^{-4}$M in CH_3CN) at λ = 469 nm upon addition of Zn^{2+}, indicating the formation of 1:1 complex.

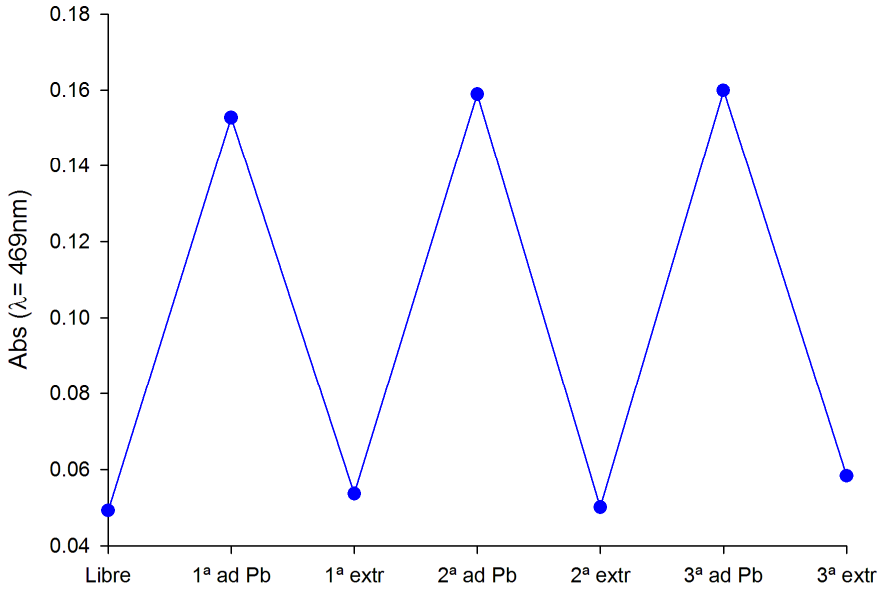

Figure SI 40. Stepwise complexation (addition of Zn^{2+}) /decomplexation (extraction with H_2O) cycles of ligand **3** ($1 \cdot 10^{-4}$ M in CH_2Cl_2) and Zn^{2+}, carried out by UV/Vis analysis.

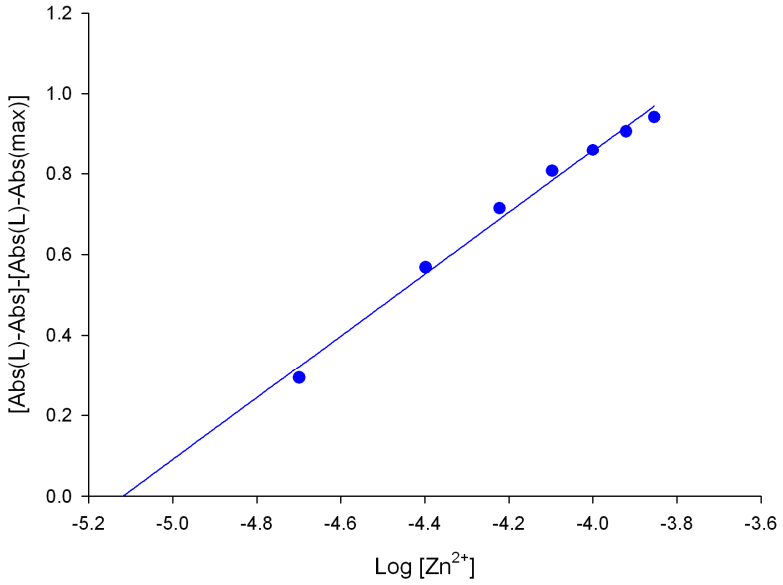

Figure SI 41. Absorbance of **3** (c = $1 \cdot 10^{-4}$M in CH_3CN) at each concentration of Zn^{2+} added, normalized between the minimum absorbance, found at zero equiv of Zn^{2+}; and the maximum absorbance, found at $[Zn^{2+}]= 7.6079 \cdot 10^{-6}$ M.

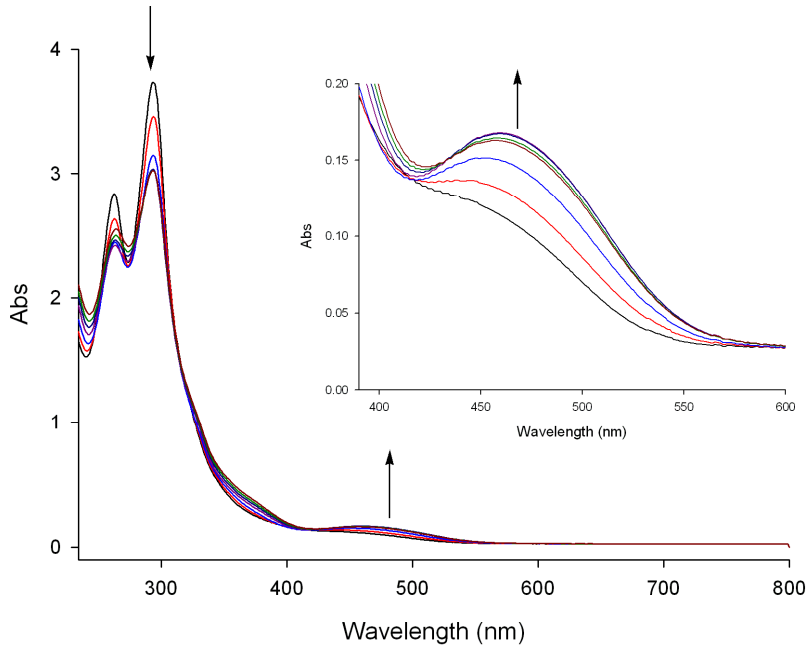

Figure SI 42. Changes in the absorption spectra of **3** (black) (c = $1 \cdot 10^{-4}$M in CH_3CN) upon addition of increasing amounts of Hg^{2+} metal cation, until 0.5 equiv was added (deep red). Arrows indicate absorption that increase or decrease during the experiment.

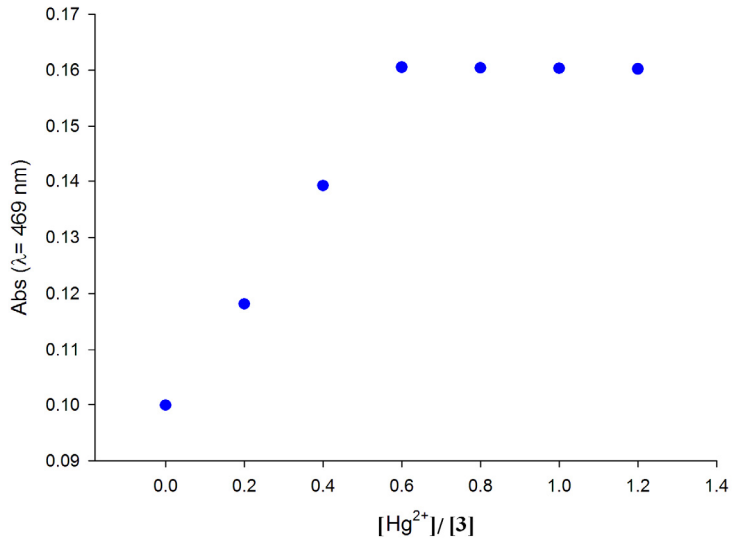

Figure SI 43. Change of absorbance of **3** (c = $1 \cdot 10^{-4}$M in CH_3CN) at λ = 469 nm upon addition of Hg^{2+}, indicating the formation of 2:1 L/M complex.

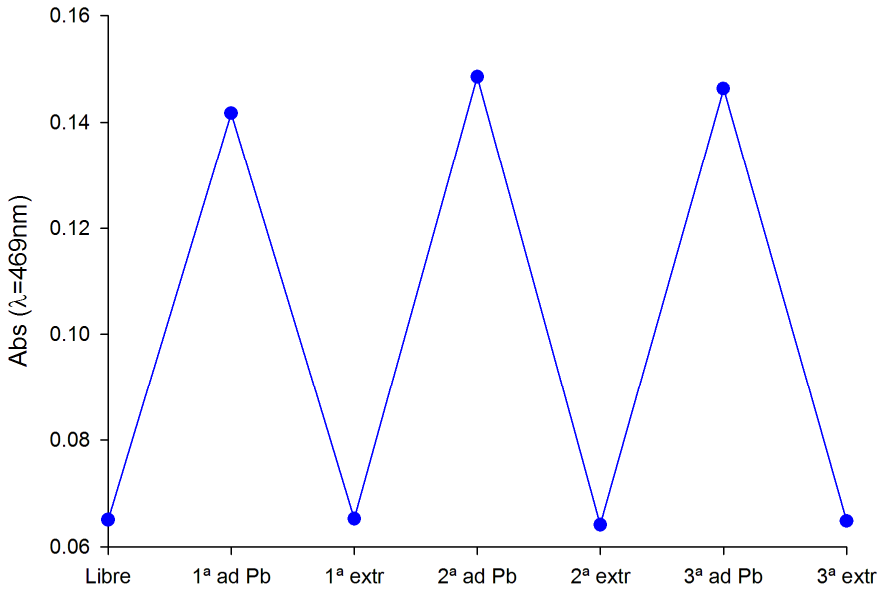

Figure SI 44. Stepwise complexation (addition of Hg^{2+}) /decomplexation (extraction with H_2O) cycles of ligand **3** ($1 \cdot 10^{-4}$ M in CH_2Cl_2) and Hg^{2+}, carried out by UV/Vis analysis.

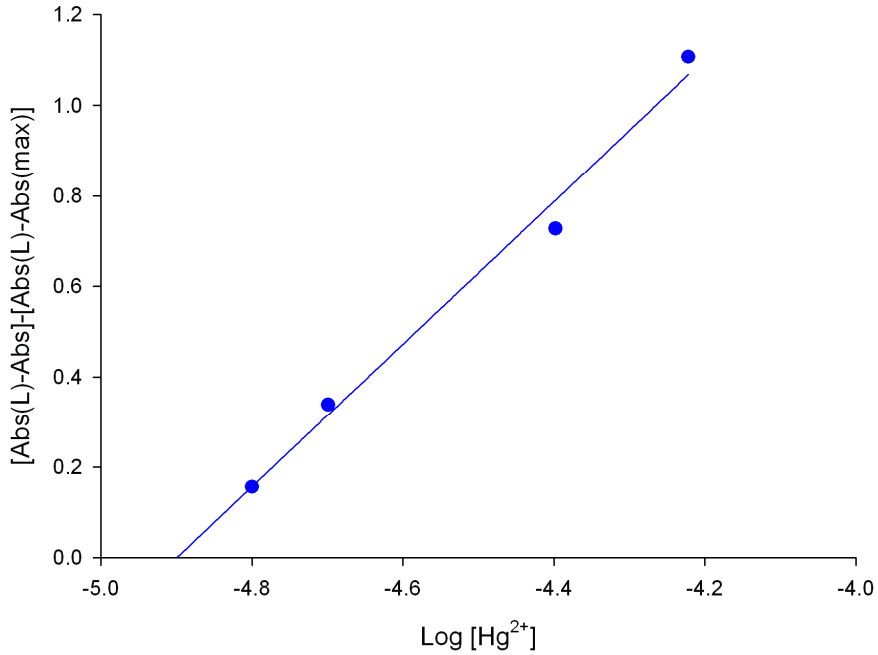

Figure SI 45. Absorbance of **3** (c = $1 \cdot 10^{-4}$M in CH_3CN) at each concentration of Hg^{2+} added, normalized between the minimum absorbance, found at zero equiv of Hg^{2+}; and the maximum absorbance, found at $[Hg^{2+}]= 1.2614 \cdot 10^{-5}$ M.

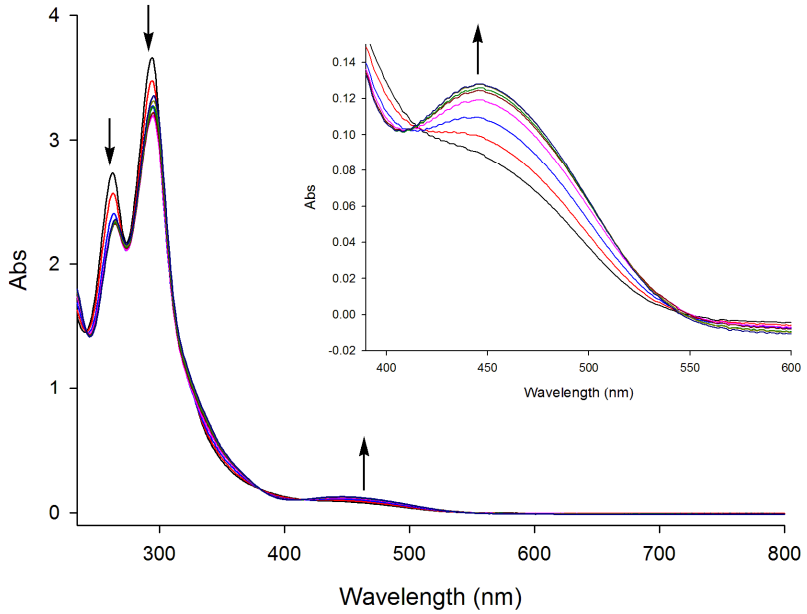

Figure SI 46. Changes in the absorption spectra of **3** (black) (c = $1 \cdot 10^{-4}$M in CH_3CN) upon addition of increasing amounts of Cd^{2+} metal cation, until 1 equiv was added (deep blue). Arrows indicate absorption that increase or decrease during the experiment.

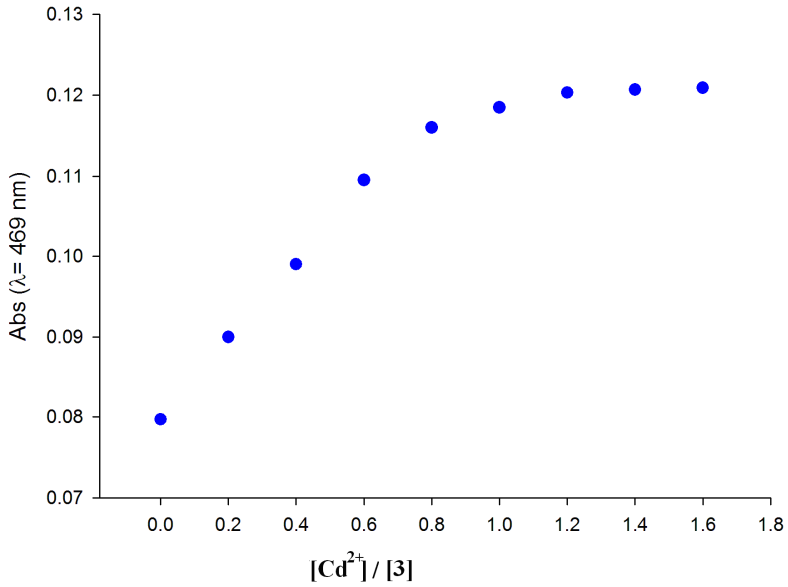

Figure SI 47. Change of absorbance of **3** (c = $1 \cdot 10^{-4}$M in CH_3CN) at λ = 469 nm upon addition of Cd^{2+}, indicating the formation of 1:1 L/M complex.

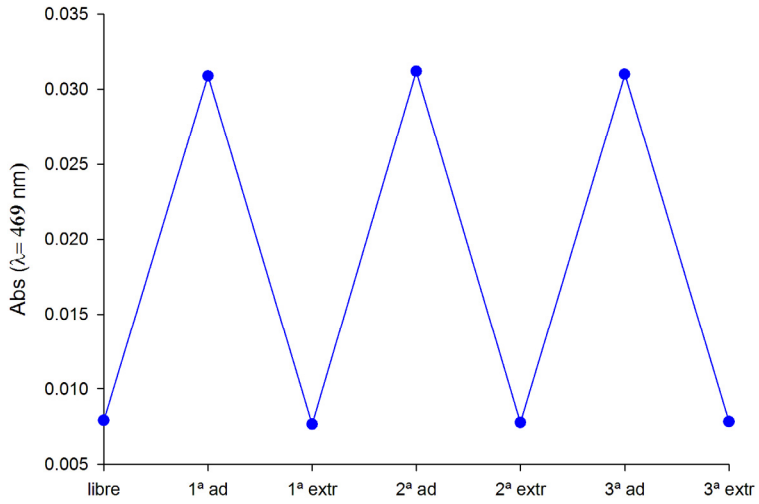

Figure SI 48. Stepwise complexation (addition of Hg^{2+}) /decomplexation (extraction with H_2O) cycles of ligand **3** ($1 \cdot 10^{-4}$ M in CH_2Cl_2) and Hg^{2+}, carried out by UV/Vis analysis.

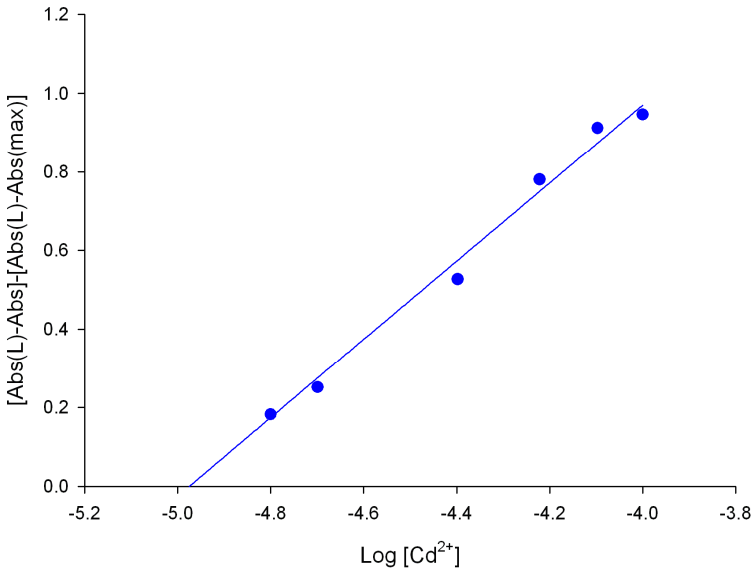

Figure SI 49. Absorbance of **3** (c = $1 \cdot 10^{-4}$M in CH_3CN) at each concentration of Cd^{2+} added, normalized between the minimum absorbance, found at zero equiv of Cd^{2+}; and the maximum absorbance, found at $[Cd^{2+}] = 1.0173 \cdot 10^{-5}$M.

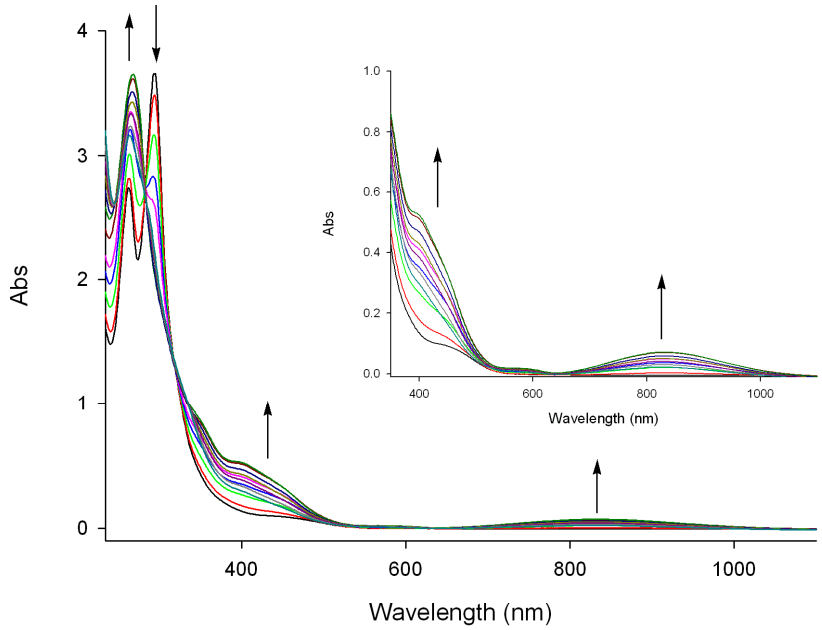

Figure SI 50. Changes in the absorption spectra of **3** (black) (1 x 10^{-4} M) in CH_3CN upon addition of increasing amounts of Cu^{2+} metal cation, until 2 equiv was added (deep cyan). Arrows indicate absorption that increase or decrease during the experiment.

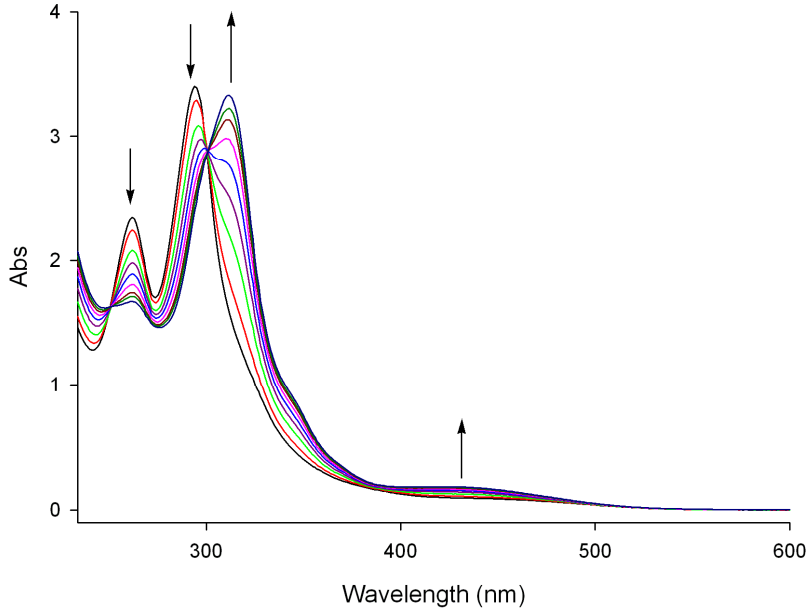

Figure SI 51. Changes in the absorption spectra of **3** (black) (c = $1 \cdot 10^{-4}$M in CH_3CN) upon addition of increasing amounts of $HP_2O_7^{3-}$ anion, until 4 equiv was added (deep blue). Arrows indicate absorption that increase or decrease during the experiment.

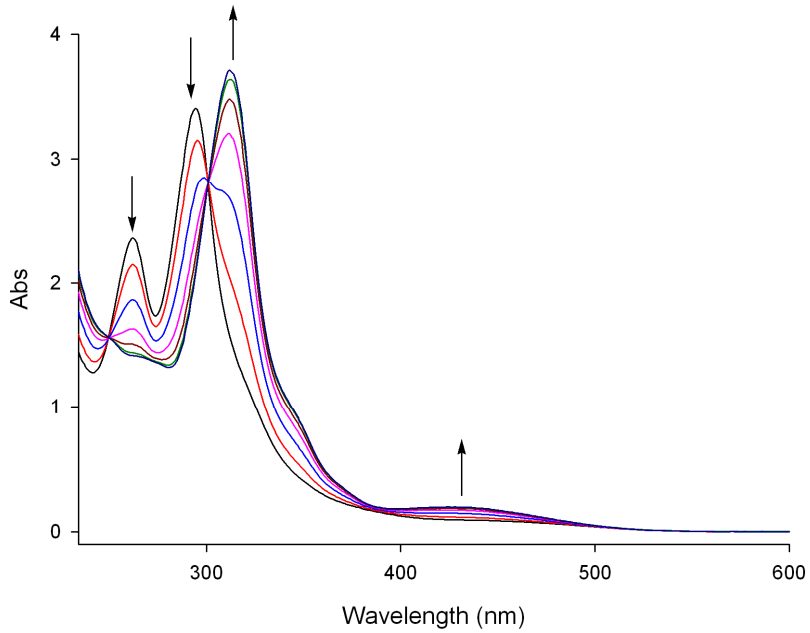

Figure SI 52. Changes in the absorption spectra of **3** (black) (c = $1 \cdot 10^{-4}$M in CH_3CN) upon addition of increasing amounts of F^- metal anion, until 3 equiv was added (deep blue). Arrows indicate absorption that increase or decrease during the experiment.

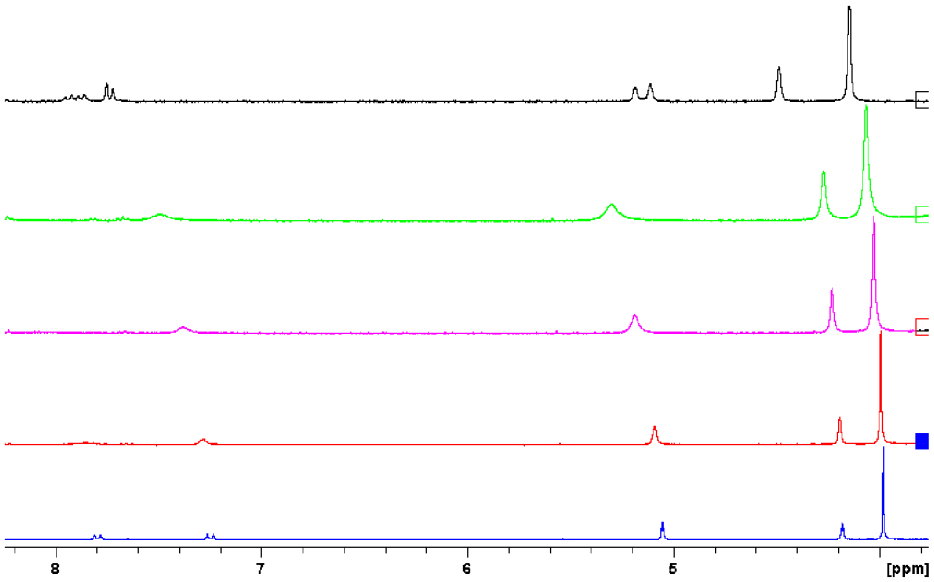

Figure SI 53. Changes in the ^{1}H-NMR spectrum of **3** (top) in acetone upon addition of increasing amounts of $HP_2O_7^{-3}$ until 2 equiv (bottom).

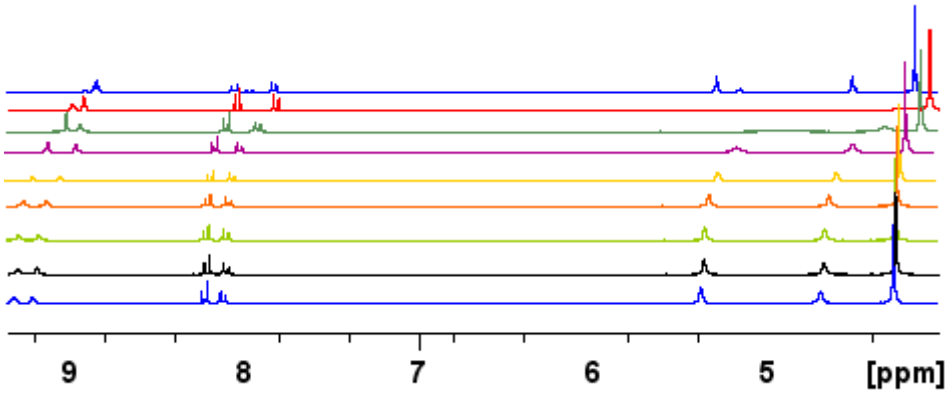

Figure SI 54. Changes in the ^{1}H-NMR spectrum of **3** (top) in acetone upon addition of increasing amounts of Pb^{2+} until 0.5 equiv (bottom).

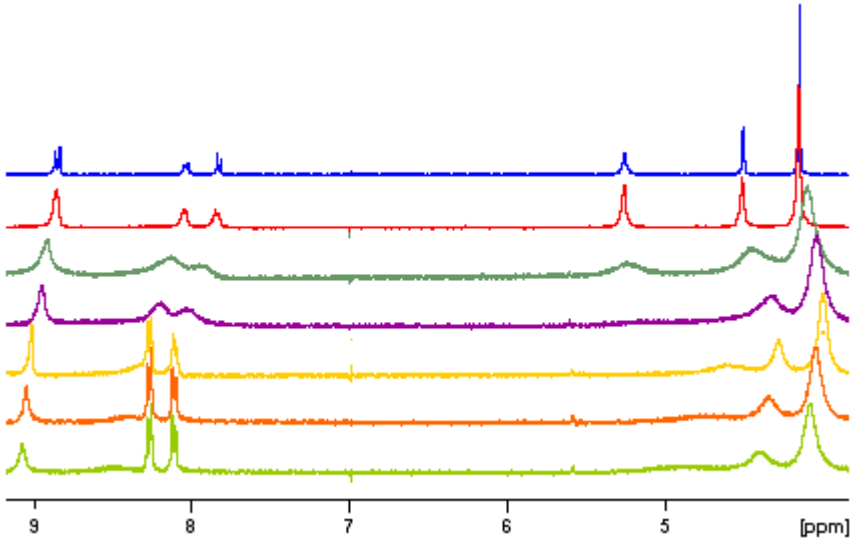

Figure SI 55. Changes in the ^{1}H-NMR spectrum of **3** (top) in acetone upon addition of increasing amounts of Zn^{2+} until 1 equiv (bottom).

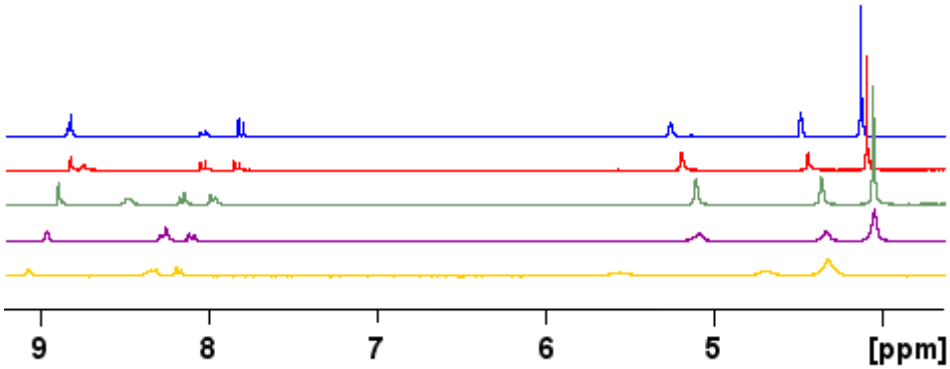

Figure SI 56. Changes in the ^{1}H-NMR spectrum of **3** (top) in acetone upon addition of increasing amounts of Hg^{2+} until 0.5 equivalent (bottom).

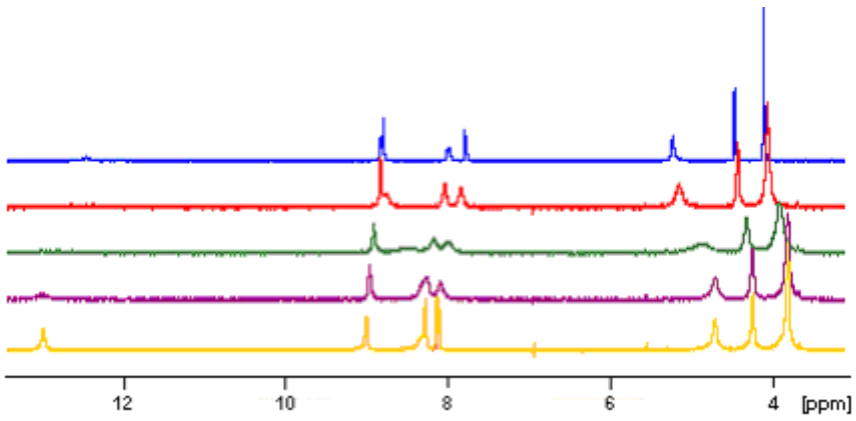

Figure SI 57. Changes in the ^{1}H-NMR spectrum of **3** (top) in acetone upon addition of increasing amounts of Cd^{2+} until 1. equiv (bottom).

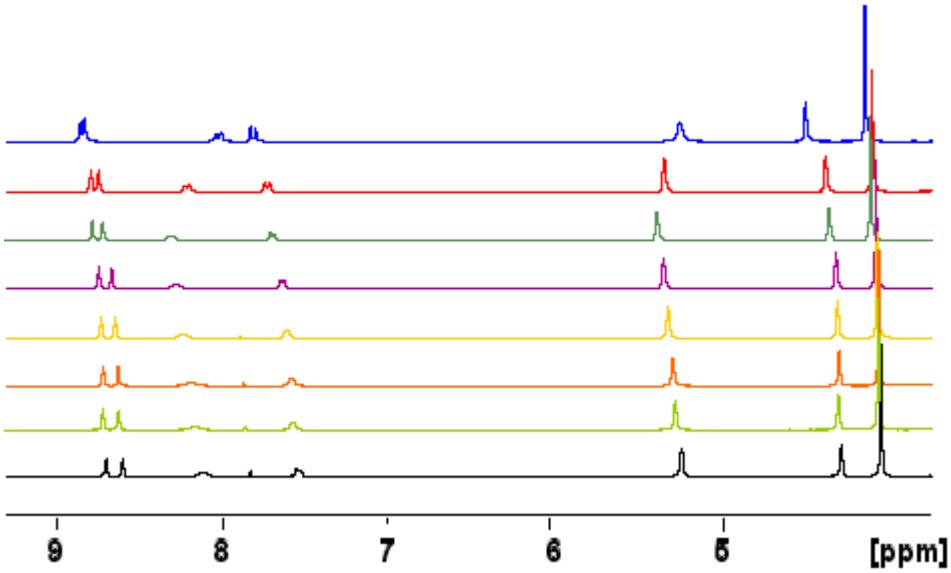

Figure SI 58. Changes in the ^{1}H-NMR spectrum of **3** (top) in acetone upon addition of increasing amounts of $HP_2O_7^{3-}$ until 1.4 equivalents (bottom).

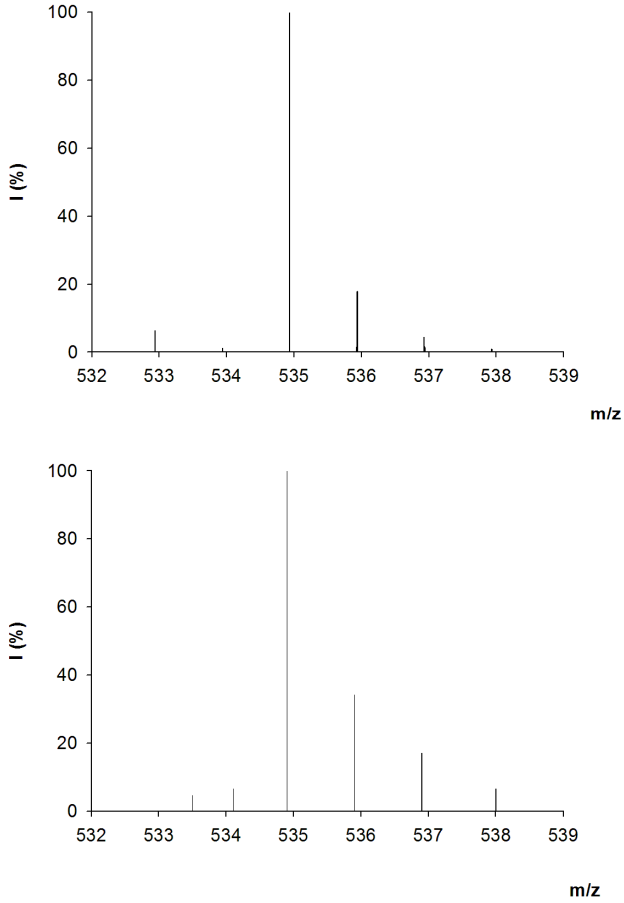

Figure SI 59. Relative abundance of the isotopic cluster for **2·HP$_2$0$_7^{3-}$** (top) experimental (in CH_3CN); (bottom) simulated.

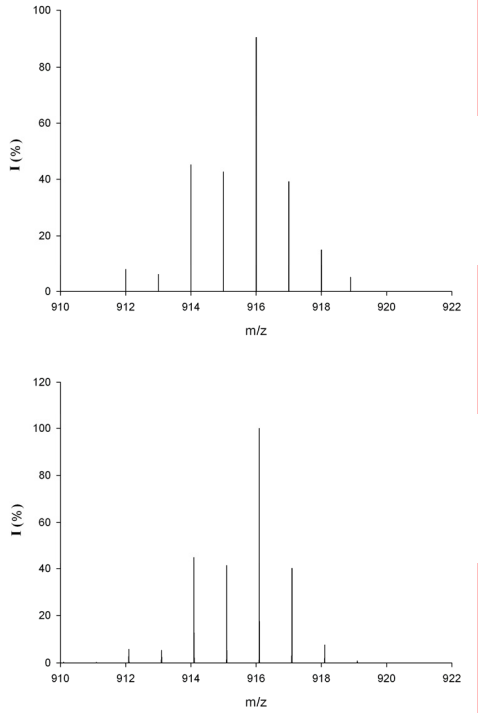

Figure SI 60. Relative abundance of the isotopic cluster for $\mathbf{3_2 \cdot Pb^{2+}}$ (top) experimental (in CH_3CN); (bottom) simulated.

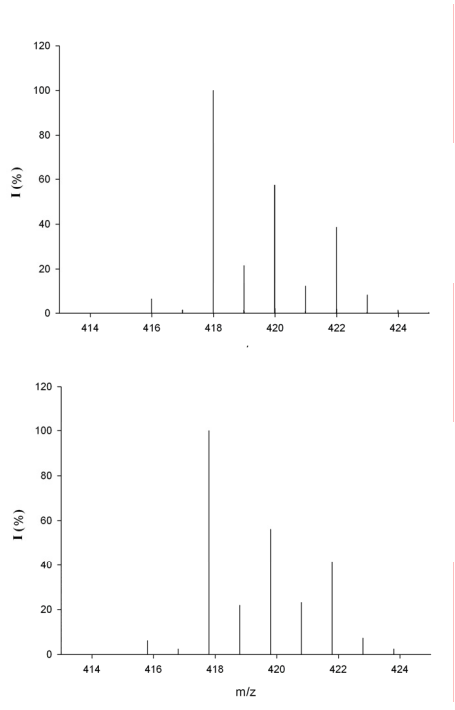

Figure SI 61. Relative abundance of the isotopic cluster for $\mathbf{3 \cdot Zn^{2+}}$ (top) experimental (in CH_3CN); (bottom) simulated.

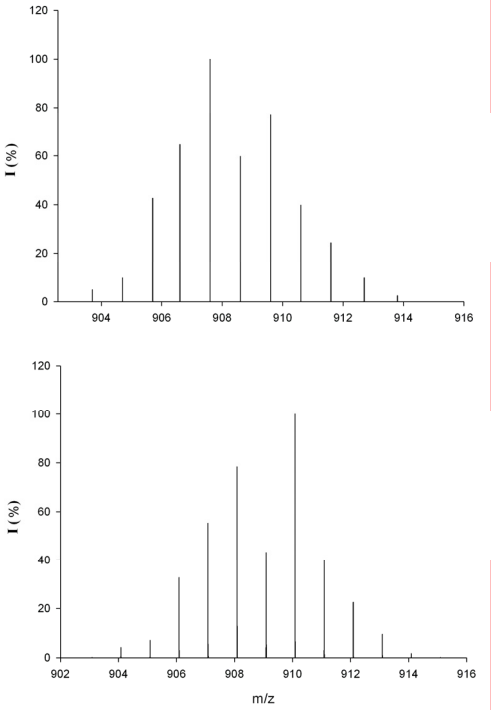

Figure SI 62. Relative abundance of the isotopic cluster for $\mathbf{3_2 \cdot Hg^{2+}}$ (top) experimental (in CH_3CN); (bottom) simulated.

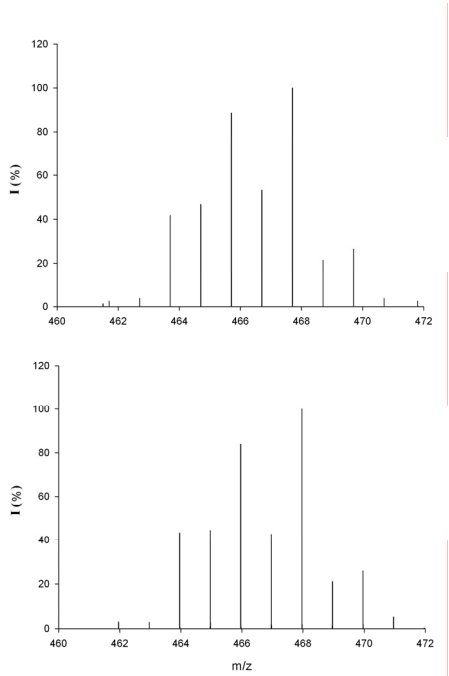

Figure SI 63. Relative abundance of the isotopic cluster for $\mathbf{3 \cdot Cd^{2+}}$ (top) experimental (in CH_3CN); (bottom) simulated.